

The role of morphology on the emergence of topologically trivial surface states and selection rules in topological-insulator nano-particles

Jorge David Castaño-Yepes^{1,*} and Enrique Muñoz^{1,2,†}

¹*Physics Institute, Pontificia Universidad Católica de Chile, Vicuña Mackenna 4860, Santiago, Chile.*

²*Research Center for Nanotechnology and Advanced-Materials CIEN-UC, Pontificia Universidad Católica de Chile, Vicuña Mackenna 4860, Santiago, Chile.*

Confined electronic states and optical transitions in 3D topological insulator nanoparticles have been studied in the literature, assuming idealized geometries such as spheres or infinitely long cylinders, that allow to obtain analytical solutions to the corresponding eigenvalue equation within such geometries. In contrast, in this article we consider triangular-shaped nanoplates as a more realistic approximation to the experimentally observed morphologies of topological insulator nanoparticles. In this particular geometry, we obtain analytical expressions for the confined eigenstates and the corresponding energy spectrum. Moreover, by a spatial representation of the probability density distribution of these states, we further identify the conditions leading to the emergence of topologically trivial surface states as a result of geometric confinement. Finally, we also study the optical transitions and the corresponding selection rules imposed by the nanoparticle size and morphology.

I. INTRODUCTION

Topological insulators (TIs) are materials presenting a large bulk band-gap, in combination with gapless topologically-protected [1] edge (in 2D TIs) or surface (in 3D TIs) states with a nearly linear (Dirac-like) dispersion, as confirmed by angle-resolved photoemission spectroscopy (ARPES) [2, 3]. Moreover, these edge/surface non-trivial topological states exhibit a remarkable spin-momentum interlocking (chirality) property [4] that makes them exciting candidates for technological applications in quantum information, spintronics and energy harvesting in thermoelectric devices [5]. The basic concept of a 2D TI was first proposed theoretically [6] and later discovered experimentally [7] in HgTe/CdTe heterostructures displaying the quantum spin Hall Effect. On the other hand, the theoretical prediction [8] of 3D TIs was rapidly followed by their experimental discovery in the $\text{Bi}_x\text{Sb}_{1-x}$ compounds [9], and since then it has triggered an active research for other materials [10] that provide actual realizations of the concept. Important examples for their relatively large band-gap [10, 11] are the metal dichalcogenides Bi_2Se_3 , Bi_2Te_3 , and Sb_2Te_3 , displaying an anisotropic crystal structure composed by stacked quintuple layers (five covalently-bonded atomic layers) stabilized by van der Waals [12] interactions. With the aid of nanofabrication techniques such as vapor-phase growth [13–16], solution-phase growth [17–19], mechanical [20–22] and chemical [23] exfoliation, these materials allow for the synthesis of TI nanostructures at different sizes and morphologies [15–17, 24–27], including nanoribbons [13, 22, 26], nanowires [14], nanorods [19, 25] and nanoplates [15–17, 24, 27] of variable thickness with sharp edges and corners.

The band structure of these materials has been accurately predicted by first-principles calculations [11], in agreement with several ARPES studies [28] that confirm the existence of well defined topologically non-trivial surface states with

Dirac-like dispersion. In addition, magnetotransport experiments [20, 21, 28–33] seem to indicate that in many TI nanostructures the charge carriers correspond to both surface and bulk electronic states [20, 28, 30, 32, 33], and that topologically protected surface states coexist and even interact with trivial surface states. The detailed mechanisms involving the coupling of bulk and trivial surface states to topologically protected surface states in such nanostructures are not fully understood yet, but are believed to originate on a combination of geometric confinement and disorder localization effects [20, 21, 28, 30, 31, 34]. In this article, we shall explore the origin of topologically trivial surface states as a consequence of morphological-dependent confinement in TI nanostructures, in order to shed some further light into such mechanisms.

A combination of band structure calculations in TIs with a full group-theoretical analysis of their symmetries [11, 35] leads to analytical effective low-energy models based on the $\mathbf{k} \cdot \mathbf{p}$ expansion near the Γ point [35]. These minimal continuum low-energy models have been used to study the confinement effects over the single-particle spectrum in 3D TI nanoparticles [36, 37] (TI-NP). Idealized geometries, such as spheres [36] and infinitely long cylindrical rods [37] have been studied so-far in the literature, and selection rules for optical transitions have been determined from analytical solutions in such cases. In these studies, geometrical confinement is mathematically enforced by a hard-wall condition [36, 37], thus demanding for the spinor eigenstates to vanish at the boundary of the domain representing the surface of the TI-NP, and hence by construction topologically trivial surface states are automatically ruled out in those analytical models. It is important to notice that, despite this is a valid boundary condition for the Schrödinger equation [38, 39], it is not the more general one for the Dirac equation. In more technical mathematical terms, this problem corresponds to the search for an appropriate self-adjoint extension of the Hamiltonian operator [40] within the domain imposed by the TI-NP geometry. Indeed, in physical terms the most general confinement condition involves the vanishing of the normal component of the probability current at the surface, as was long ago dis-

* jcastano@fis.uc.cl

† munozt@fis.puc.cl

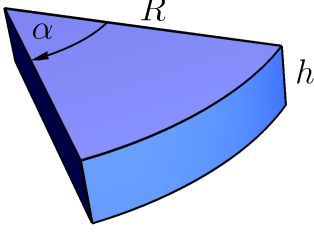


FIG. 1: Sketch of the triangular-shaped TI nanoparticle of radius R and height h , with a wedge angle α .

cussed in the context of the M.I.T bag model [41–44], and this does not necessarily imply for the whole spinor eigenstate to vanish as well, as assumed in the hard-wall boundary condition applied in previous models [36, 37]. Since the effective low-energy Hamiltonian that better describes TI-NPs [11, 35] involves a combination of linear (Dirac-like) and quadratic (Schrödinger-like) in momentum dispersions, it is important to obtain the corresponding mathematical expression for the probability current, in order to identify the appropriate boundary condition that determines confinement in the more general sense, given the morphological features of the TI-NP boundary.

In this work, we shall focus on TI-NPs with triangular shapes, as depicted in Fig. 1, as an approximation to some of the experimental morphologies observed in TI nanoplates involving sharp wedge angles [15–17, 24, 25, 27]. For this particular geometry, we define the thickness by h , the radius by R and the wedge angle by α . Our goal is to investigate the energy spectrum of the confined bulk states within such TI-NPs, as well as the corresponding probability density distribution, in order to identify the morphological features leading to the presence of topologically trivial surface states. We shall also study the corresponding selection rules for optical transitions between such confined states. For this purpose, as we further show, we developed an exact analytical solution to the eigenvalue problem, that allows us to investigate the scaling of the spectrum, density distribution and transition probabilities as a function of the morphological confinement parameters. Finally, using our explicit analytical solutions, we explore the features of a TI-NP with the shape of a very long cylindrical rod [19, 25] in the limit $\alpha \rightarrow 2\pi$, $h \rightarrow \infty$.

II. THE BULK HAMILTONIAN

We are interested in the study of confined electronic states within a TI-NP, whose geometry is depicted in Fig. 1, and hence we start from the corresponding bulk Hamiltonian for the material. For this purpose, we consider a low-energy continuum model that represents the band structure of a typical topological insulator near the Γ -point [11, 35, 36]:

$$\hat{\mathcal{H}} = \left(\frac{\Delta_0}{2} + \frac{\gamma}{k_\Delta} \mathbf{k}^2 \right) \tau_z \otimes \sigma_0 + \gamma (k_\tau \tau_x \otimes \sigma_z + k_- \tau_x \otimes \sigma_+ + k_+ \tau_x \otimes \sigma_-), \quad (1)$$

where we have taken into account the spin (σ) and pseudo-spin (τ) degrees of freedom. Here, we defined the momentum operators $\mathbf{k} = (k_x, k_y, k) = -i\nabla$, $k_\pm = k_x \pm ik_y$, as well as the ladder spin operators $\sigma_\pm = (\sigma_x \pm i\sigma_y)/2$. The numerical values for the parameters Δ_0 , γ , and k_Δ are presented in Table I for three different TI materials.

Based on this Hamiltonian model for the bulk, we incorporate the confinement effects induced by the specific TI-NP geometry by imposing a current insulating condition at the surface [41–44]. For a confined state, only the *normal* component of the current $\mathbf{n} \cdot \mathbf{J}|_{\partial\Omega}$ determines the net probability flux through the boundary $\partial\Omega$, and therefore it must vanish at each of the surfaces depicted in Fig. 1, i.e. at $\phi = \{0, \alpha\}$, $z = \{0, h\}$, and $r = R$. The later yields quantization conditions, as we shall discuss in further detail, and the correct identification of the probability density at the surface of the system. In order to simplify the mathematical notation, and further algebraic manipulations, we define the “mass” differential operator

$$\mathbb{M}(\mathbf{k}) \equiv \frac{\Delta_0}{2} + \frac{\gamma}{k_\Delta} \mathbf{k}^2, \quad (2)$$

so that the Hamiltonian Eq. (1) can be written in the alternative and more compact form

$$\hat{\mathcal{H}} = \mathbb{M}(\mathbf{k}) \hat{\beta} + \gamma (\boldsymbol{\alpha} \cdot \mathbf{k}), \quad (3)$$

where we defined the Dirac 4×4 matrices in the standard representation

$$\boldsymbol{\alpha} = \begin{pmatrix} 0 & \boldsymbol{\sigma} \\ \boldsymbol{\sigma} & 0 \end{pmatrix}, \quad \hat{\beta} = \begin{pmatrix} \mathbb{1} & 0 \\ 0 & -\mathbb{1} \end{pmatrix}. \quad (4)$$

Therefore, with the purpose of studying the energy spectrum and confined states within the nanoparticle, we investigate the eigenvalue problem $\hat{\mathcal{H}}\Psi(r, \phi, z) = E\Psi(r, \phi, z)$, where $\Psi = (\varphi, \chi)^T$ is a 4-component spinor. This eigenvalue problem, according to the matrix structure in Eq. (3), leads to the coupled system of differential equations

$$[\mathbb{M}(\mathbf{k}) - E] \varphi + \gamma (\boldsymbol{\sigma} \cdot \mathbf{k}) \chi = 0, \quad (5a)$$

$$\gamma (\boldsymbol{\sigma} \cdot \mathbf{k}) \varphi - [\mathbb{M}(\mathbf{k}) + E] \chi = 0. \quad (5b)$$

Based on the explicit analytical solutions obtained for the constant mass limit $\mathbb{M}(\mathbf{k}^2) \rightarrow \Delta_0/2$ (see Sec. 2 in Supplemental material for details), we solve the general case by the spinors

$$\varphi = e^{ikz} \begin{pmatrix} c_1 e^{ij\phi} J_j(\kappa r) \\ c_2 e^{i(j+1)\phi} J_{j+1}(\kappa r) \end{pmatrix}, \quad (6a)$$

$$\chi = e^{ikz} \begin{pmatrix} c_3 e^{ij\phi} J_j(\kappa r) \\ c_4 e^{i(j+1)\phi} J_{j+1}(\kappa r) \end{pmatrix}, \quad (6b)$$

where $J_j(x)$ are Bessel functions of order j , and κ is a real constant, to be determined as a function of the energy E , as follows.

Material	Δ_0 (eV)	γ (eV Å)	k_Δ (Å ⁻¹)	R_0 (Å)
Bi ₂ Se ₃ [45]	-0.338	2.2	0.13	1.3
Bi ₂ Te ₃ [35]	-0.3	2.4	0.026	0.81
Pb _{0.81} Sn _{0.19} Se [46]	-0.025	3.2	0.2	26

TABLE I: Parameters for the bulk Hamiltonian Eq. (1) for different topological materials, after Refs. [35, 45, 46].

By inserting the spinors Eq. (6) into Eq. (5a) and Eq. (5b), we obtain the algebraic linear system

$$\mathbb{A}(\kappa, E)\mathbf{c} = 0, \quad (7)$$

where we defined the vector $\mathbf{c} = (c_1, c_2, c_3, c_4)^T$, as well as the matrix

$$\mathbb{A}(\kappa, E) = \begin{bmatrix} \Lambda - E & 0 & k\gamma & -i\kappa\gamma \\ 0 & \Lambda - E & i\kappa\gamma & -k\gamma \\ k\gamma & -i\kappa\gamma & -(\Lambda + E) & 0 \\ i\kappa\gamma & -k\gamma & 0 & -(\Lambda + E) \end{bmatrix}. \quad (8)$$

Here, we also defined the coefficient

$$\Lambda = \frac{\Delta_0}{2} + \frac{\gamma}{k_\Delta} (k^2 + \kappa^2). \quad (9)$$

The linear system is solvable if $\det \mathbb{A} = 0$, which implies the secular equation

$$[\Lambda^2 - E^2 + \gamma^2(k^2 + \kappa^2)]^2 = 0, \quad (10)$$

whose solutions are the energy eigenvalues as a function of κ

$$E_{\pm} = \pm \sqrt{\left(\frac{\Delta_0}{2} + \frac{\gamma}{k_\Delta} (k^2 + \kappa^2)\right)^2 + \gamma^2(k^2 + \kappa^2)}. \quad (11)$$

A. Spinor eigenvectors and energy spectrum

The linear system defined by Eq. (7) possesses four independent eigenvectors defined by the coefficients $\mathbf{c} = (c_1, c_2, c_3, c_4)^T$, as follows

$$\begin{pmatrix} i \frac{\kappa(-\Lambda \pm \sqrt{\Lambda^2 + \gamma^2(k^2 + \kappa^2)})}{\gamma(k^2 + \kappa^2)} \\ \frac{k(-\Lambda \pm \sqrt{\Lambda^2 + \gamma^2(k^2 + \kappa^2)})}{\gamma(k^2 + \kappa^2)} \\ 0 \\ 1 \end{pmatrix}, \begin{pmatrix} \frac{k(\Lambda \pm \sqrt{\Lambda^2 + \gamma^2(k^2 + \kappa^2)})}{\gamma(k^2 + \kappa^2)} \\ i \frac{\kappa(\Lambda \pm \sqrt{\Lambda^2 + \gamma^2(k^2 + \kappa^2)})}{\gamma(k^2 + \kappa^2)} \\ 1 \\ 0 \end{pmatrix}. \quad (12)$$

By construction, these four solutions are clearly degenerated by pairs, as seen in Eq. (11). However, we still must determine the explicit values for the parameters κ , k , and j , and here is where the geometrical confinement effects come into place. We show that the probability current associated to

the Hamiltonian Eq. (1) is given by the expression (see Sec. 1 in Supplemental for details)

$$\mathbf{J} = \frac{i\gamma}{k_\Delta} [\nabla \Psi^\dagger (\tau_z \otimes \sigma_0) \Psi - \Psi^\dagger (\tau_z \otimes \sigma_0) \nabla \Psi] + \Psi^\dagger \boldsymbol{\alpha} \Psi, \quad (13)$$

where the first contribution arises from the quadratic dispersion terms in the Hamiltonian, and hence is reminiscent from the standard Schrödinger expression, while the second term arises from the linear terms, leading to a Dirac pseudo-relativistic expression.

As we already pointed out, the mathematical condition representing quantum confinement of the electronic eigenstates within the TI-NP is that the normal current at the boundary $\partial\Omega$ vanishes, i.e. $\mathbf{n} \cdot \mathbf{J}|_{\partial\Omega} = 0$. By imposing this condition at the surfaces $z = 0$ and $z = h$, i.e. $\hat{\mathbf{e}}_z \cdot \mathbf{J}|_{z=\{0,h\}} = 0$, we are led to construct linear combinations from the basic solutions of the form $e^{ikz} - e^{-ikz} \propto \sin(kz)$, to obtain a quantization of the z -component of the momentum k

$$k = \frac{m\pi}{h}, \quad m = 1, 2, \dots \quad (14)$$

The analogous condition at the lateral surfaces of the wedge $\phi = 0$ and $\phi = \alpha$, i.e. $\hat{\mathbf{e}}_\phi \cdot \mathbf{J}|_{\phi=\{0,\alpha\}} = 0$, leads to linear combinations of the basic solutions of the form $e^{ij\phi} - e^{-ij\phi} \propto \sin(j\phi)$, with the corresponding quantization of the index j

$$j = \frac{l\pi}{\alpha}, \quad l = 1, 2, \dots \quad (15)$$

By incorporating the quantization conditions Eq. (14) and Eq. (15), in order to simplify the notation, let us define the coefficients

$$\mathcal{M} = \frac{\Lambda}{\gamma(k^2 + \kappa^2)}, \quad \widetilde{\mathcal{M}} = \frac{\sqrt{\Lambda^2 + \gamma^2(k^2 + \kappa^2)}}{\gamma(k^2 + \kappa^2)}, \quad (16)$$

such that the four independent states, combining Eq. (12) and Eq. (6), are given by:

$$\langle \mathbf{r} | nml; 1^\pm \rangle = \sin(kz) \sin(j\phi) \times \begin{pmatrix} i\kappa(-\mathcal{M} \pm \widetilde{\mathcal{M}})J_j(\kappa r) \\ k(-\mathcal{M} \pm \widetilde{\mathcal{M}})J_{j+1}(\kappa r)e^{i\phi} \\ 0 \\ J_{j+1}(\kappa r)e^{i\phi} \end{pmatrix}, \quad (17a)$$

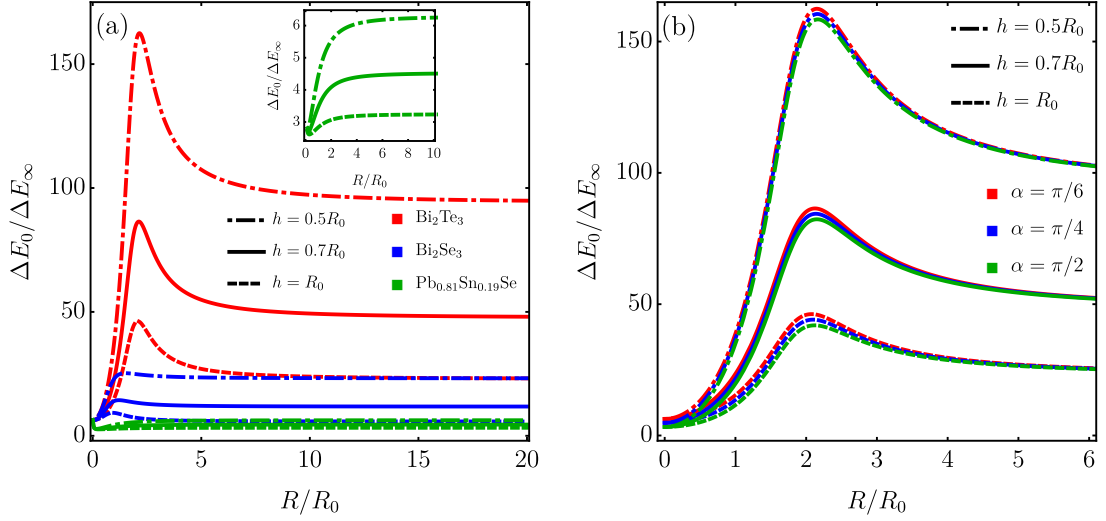


FIG. 2: Energy gap for TI nanoparticles of different materials, as a function of the morphological parameters α , h , and R . (a) Bi_2Te_3 , Bi_2Se_3 , and $\text{Pb}_{0.81}\text{Sn}_{0.19}\text{Se}$, respectively, at fixed $\alpha = \pi/6$. The inset shows the impact of the material parameters on the energy scaling for $\text{Pb}_{0.81}\text{Sn}_{0.19}\text{Se}$. (b) Bi_2Te_3 for three different values of $\alpha = \pi/6$, $\pi/4$, and $\pi/2$, respectively. Here $R_0 = 2\gamma/|\Delta_0|$ and ΔE_∞ is given by Eq. (22).

$$\langle \mathbf{r} | nml; 2^\pm \rangle = \sin(kz) \sin(j\phi) \times \begin{pmatrix} k(\mathcal{M} \pm \tilde{\mathcal{M}})J_j(\kappa r) \\ i\kappa(\mathcal{M} \pm \tilde{\mathcal{M}})J_{j+1}(\kappa r)e^{i\phi} \\ J_j(\kappa r) \\ 0 \end{pmatrix}, \quad (17b)$$

and the general solution can be written as the linear combination

$$|nml\rangle = \sum_{s=\pm} [A_s |nml, 1^s\rangle + B_s |nml, 2^s\rangle]. \quad (18)$$

Finally, imposing the confinement condition at the external radial surface $r = R$, i.e. $\hat{\mathbf{e}}_r \cdot \mathbf{J}|_{r=R} = 0$ leads to the equation

$$J_{\frac{l\alpha}{\alpha}}(\kappa R)J_{\frac{l\alpha}{\alpha}+1}(\kappa R) = 0, \quad (19)$$

where the quantization condition Eq. (15) over j was explicitly implemented in terms of the integer l .

Therefore, if $\kappa_{nl} = \kappa R$ are the (infinitely many) roots of Eq. (19), the energy eigenvalues for the confined electronic states are given by the explicit analytical expression

$$E_{nml}^\pm = \pm \left[\left[\frac{\Delta_0}{2} + \frac{\gamma}{k_\Delta} \left(\frac{m^2\pi^2}{h^2} + \frac{\kappa_{nl}^2}{R^2} \right) \right]^2 + \gamma^2 \left(\frac{m^2\pi^2}{h^2} + \frac{\kappa_{nl}^2}{R^2} \right) \right]^{1/2}. \quad (20)$$

It is interesting to remark that this expression, in the limit of $h \rightarrow \infty$, restores the continuum limit for the z -component of the linear momentum (see also Eq. (14)). Moreover, as $\alpha \rightarrow 2\pi$ the wedge becomes a full cylinder, and as seen in Eq. (15)

the usual total angular momentum quantization is restored, as j is either an integer or half-integer in this limit, i.e. $j \rightarrow l - 1/2$ for $l = 0, \pm 1, \pm 2, \dots$, and $\sin(j\phi) \rightarrow e^{\pm i(l-1/2)\phi}$. Therefore, in the limit of a full ($\alpha \rightarrow 2\pi$) infinitely long ($h \rightarrow \infty$) cylinder, the quantization condition Eq. (19) reduces to

$$J_{l-1/2}(\tilde{\kappa}R)J_{l+1/2}(\tilde{\kappa}R) = 0. \quad (21)$$

Let us define the energy gap for the infinitely long full cylinder by the expression

$$\begin{aligned} \Delta E_\infty &= \lim_{\substack{h \rightarrow \infty \\ \alpha \rightarrow 2\pi}} (E_{1,0,0}^+ - E_{1,0,0}^-) \\ &= 2\sqrt{\left[\frac{\Delta_0}{2} + \frac{\gamma}{k_\Delta} \left(\frac{\tilde{\kappa}_{10}}{R} \right)^2 \right]^2 + \gamma^2 \left(\frac{\tilde{\kappa}_{10}}{R} \right)^2}. \end{aligned} \quad (22)$$

In Fig. 2, we represent the energy gap $\Delta E_0 = E_{1,1,1}^+ - E_{1,1,1}^-$, defined as the difference between the lowest unoccupied and highest occupied energy levels, normalized by the corresponding ΔE_∞ , as a function of the particle radius, in units of the "Compton wavelength" $R_0 = 2\gamma/|\Delta_0|$. We compare the energy gap for three different TI materials, Bi_2Te_3 , Bi_2Se_3 , and $\text{Pb}_{0.81}\text{Sn}_{0.19}\text{Se}$, respectively, as a function of the TI-NP height h (in units of R_0) (Fig. 2(a)), and for different values of the wedge angle α (Fig. 2(b)). From Fig. 2(a), it is evident that the TI-NP gap is extremely sensitive to the specific material parameters, specially the size of the bulk gap Δ_0 , which is comparatively larger for Bi_2Te_3 . It is also clear that the confinement in the z -direction, represented by the TI-NP thickness h is the most relevant at determining the size of the gap, as seen in both Fig. 2(a,b). In particular, Fig. 2(b) shows that the gap is very weakly dependent on the wedge angle α . In all three examples, the changes in the TI morphology increases the energy gap (as compared with the infinite long

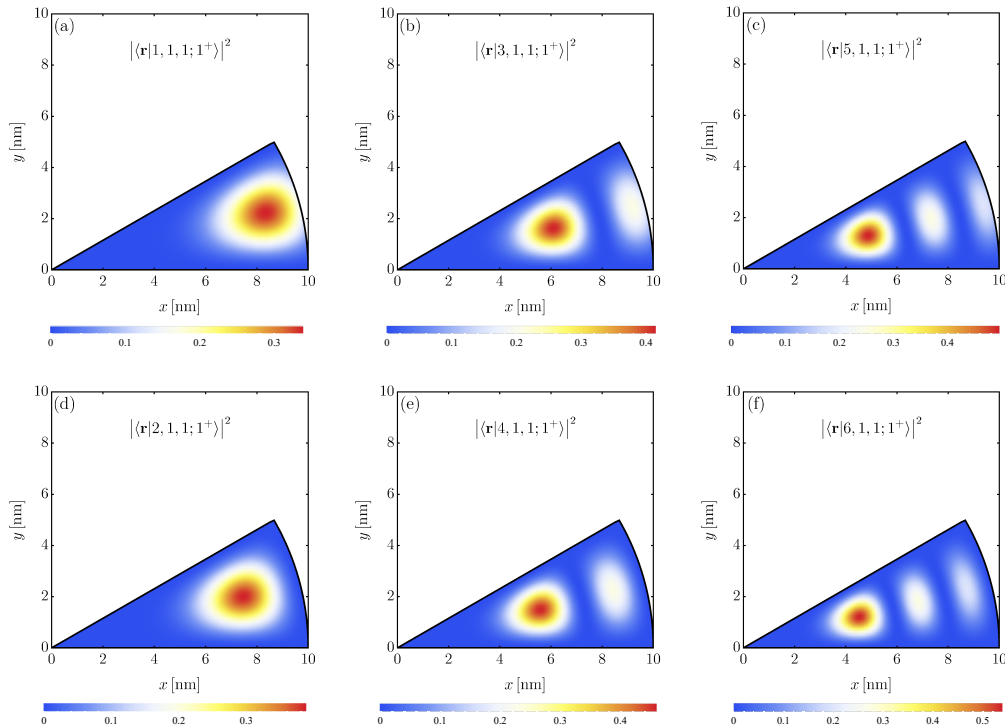


FIG. 3: Probability density, represented as a 2D-color plot at the plane $z = 0.5h$, for different confined states within a TI nanoparticle with $\alpha = \pi/6$, $l = m = 1$, and $1 \leq n \leq 6$.

cylindrical rod) up to two orders of magnitude for the material constants considered in Table I.

III. THE PROBABILITY DENSITY AND TOPOLOGICALLY TRIVIAL SURFACE STATES

From the analytical solutions obtained for the spinor eigenstates presented in the previous section, it is straightforward to calculate the probability density distribution (for $q = 1, 2$), as $\rho_{nml, q^\pm}(\mathbf{r}) = |\langle \mathbf{r} | nml, q^\pm \rangle|^2$. This function provides a clear image of the spatial localization of each spinor eigenstate within the TI-NP and, in particular, it allows us to investigate the conditions leading to the emergence of topologically trivial surface states. In Fig. 3, we represent the probability density for different confined states in a TI-NP with $\alpha = \pi/6$, at the horizontal plane $z = 0.5h$, for $q = 1$, $l = m = 1$, and $1 \leq n \leq 6$. We notice that the states with odd n exhibit a finite probability density at the surface of the nanoparticle. A complementary analysis is presented in Fig. 4, where the density distribution can be appreciated in 3D. Clearly, the number of maxima along the z -direction is determined by the corresponding quantum number m . In contrast, it can be shown that states with $q = 2$ exhibit states at the surface for n even, but with a lower probability density, as is depicted in Fig. 5.

In Fig. 6, we study the effect of the angular momentum quantum number l , characterizing the confinement effect due to the wedge angle $\alpha = \pi/6$ for this example. It is clear from

Fig. 6 that the number of nodes exhibited by the probability density distribution in the polar angular direction is given by the integer l , as seen for the examples $l = 2$ in Fig. 6(a-c) and $l = 3$ in Fig. 6(d-f), respectively. Again we observe, in all six cases with odd n ($n = 1, 2, 3$), the presence of a finite probability density at the surface of the TI-NP. For completeness, in order to study the impact of the geometry on the eigenstates, Fig. 7 shows the role of α on the spatial distribution of the probability density. We chose the angles $\alpha = \pi/2$ and π , and different values of n and l for $m = 1$, which follows the same properties already discussed for the case $\alpha = \pi/6$.

In Fig. 8, we analyze the effect of the index $s = \pm$, by comparing the probability density distribution of the states $|nml; 1^+\rangle$ and $|nml; 1^-\rangle$, respectively, as a function of the radial coordinate at the plane $z = 0.5h$ for a TI-NP with a wedge angle $\alpha = \pi/6$. Fig. 8(a) corresponds to the state with $n = l = m = 1$, along the symmetry plane $\phi = \alpha/2$ as shown in the dashed line on the inset. On the other hand, Fig. 8(b) corresponds to the state with $n = 3$, $m = 1$, and $l = 2$, along the symmetry plane $\phi = \alpha/4$, as shown in the dashed line on the corresponding inset. Clearly, in both examples we observe the presence of a finite probability density at the surface of the TI-NP, but with different amplitude, given that the weight factors for each state are different.

Our analysis shows that the morphology of the TI nanoparticle as well as the values of the quantum numbers implies the existence of spatial regions with topologically trivial surface states. In general terms, depending on the parity of n the quantum state $|nml, q^s\rangle$ has $m \times l$ regions in the surface $r = R$

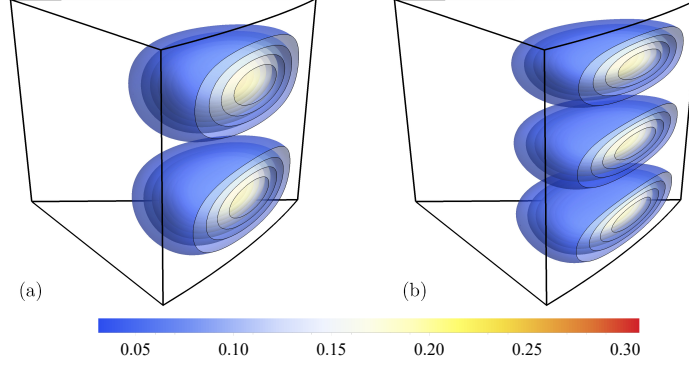


FIG. 4: Probability density of the state $|1, m, 1; 1^+\rangle$ for (a) $m = 2$ and (b) $m = 3$ with $\alpha = \pi/6$.

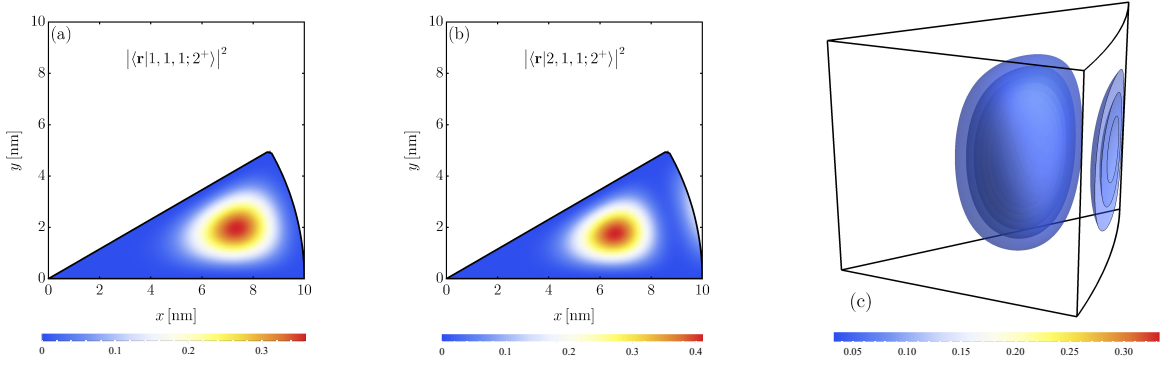


FIG. 5: Probability density of the state $|n, 1, 1; 2^+\rangle$ for (a) $n = 1$ and (b) $n = 2$ with $\alpha = \pi/6$ at $z = 0.5h$. In order to appreciate the surface state, panel (c) is the 3D reconstruction for $|\langle \mathbf{r} | 2, 1, 1; 2^+\rangle|^2$.

where localized fermionic states can be found.

IV. OPTICAL TRANSITIONS AND SELECTION RULES

In this section, we analyze the optical transitions, along with the corresponding selection rules, within the standard dipolar approximation for the electric field. For this purpose, we consider the matrix elements of the total electric dipole operator [37, 47]

$$\mathbf{d} = e\mathbf{r}(\tau_0 \otimes \sigma_0) + \frac{eR_0}{2}(\tau_y \otimes \boldsymbol{\sigma}), \quad (23)$$

where the first term represents the intra-band contribution, arising from the envelope wavefunctions multiplying the same basis state in the $\mathbf{k} \cdot \mathbf{p}$ approximation for the bulk band structure [36, 37, 47]. On the other hand, the second term in Eq. (23) accounts for transitions between different $\mathbf{k} \cdot \mathbf{p}$ basis states [36, 37, 47].

Let us define the probability amplitude for an optical transition along the $\hat{\mathbf{e}}_\mu$ -direction, by the matrix element

$$T_\mu(|i\rangle \rightarrow |f\rangle) = \langle n'm'l'; f | \hat{\mathbf{e}}_\mu \cdot \mathbf{d} | nml; i \rangle, \quad (24)$$

where i, f denotes each of the four possible eigenstates labelled by the indexes $q = 1, 2$ and $s = \pm$, as defined in the

previous section. We shall discuss our analytical results for the transition amplitudes in different orthogonal directions.

A. Transition amplitudes in z-direction

Let us first consider the transition amplitude in the z-direction, given by the analytical expression

$$\begin{aligned} T_z(|1^\pm\rangle \rightarrow |1^\pm\rangle) &= \frac{e\alpha}{2} A_\pm A'_\pm \delta_{ll'} \\ &\times \left\{ \kappa\kappa' \left(-\mathcal{M} \pm \widetilde{\mathcal{M}} \right) \left(-\mathcal{M}' \pm \widetilde{\mathcal{M}}' \right) I_n^{n'} I_z(\Delta m, M) \right. \\ &+ \left[k\kappa' \left(-\mathcal{M} \pm \widetilde{\mathcal{M}} \right) \left(-\mathcal{M}' \pm \widetilde{\mathcal{M}}' \right) + 1 \right] \widetilde{I}_n^{n'} I_z(\Delta m, M) \\ &\left. + \frac{i\hbar R_0}{4} \delta_{mm'} \left[k' \left(-\mathcal{M}' \pm \widetilde{\mathcal{M}}' \right) - k \left(-\mathcal{M} \pm \widetilde{\mathcal{M}} \right) \right] \widetilde{I}_n^{n'} \right\}, \end{aligned} \quad (25)$$

where the coefficients $I_n^{n'}$ and $\widetilde{I}_n^{n'}$ are defined in Sec.4 of the Supplemental. In particular, for $\Delta m = m' - m$ and $M = m' + m$, the coefficient $I_z(\Delta m, M)$, defined by the analytical expression

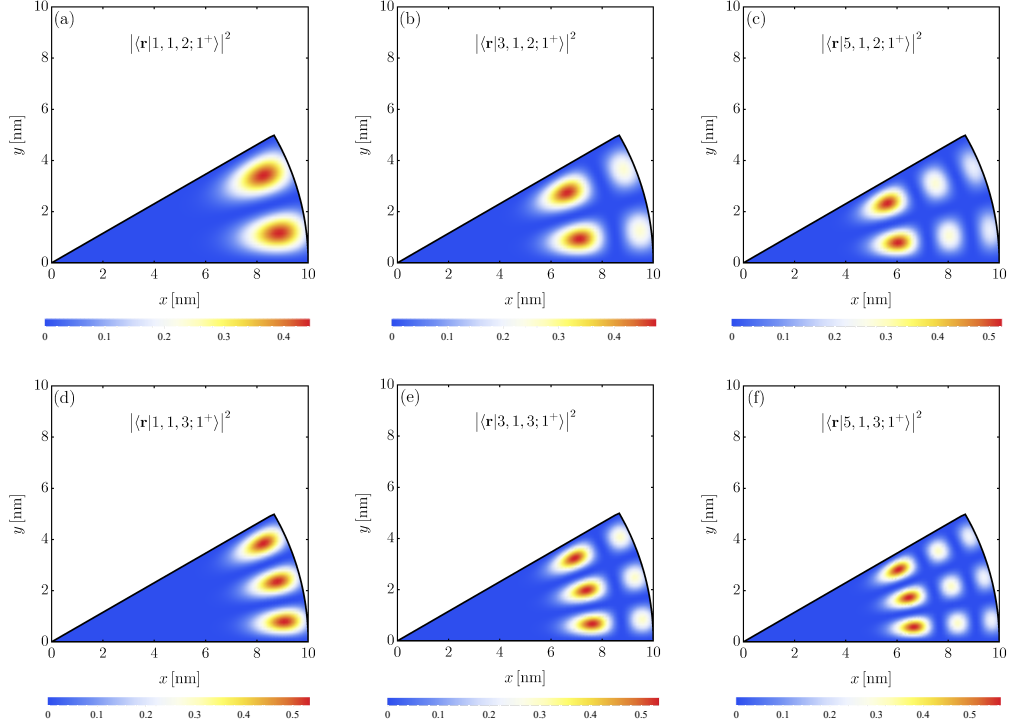


FIG. 6: Probability density, represented as a 2D-color plot at the plane $z = 0.5h$, for different confined states within a TI nanoparticle with $\alpha = \pi/6$, $m = 1$, and $n = 1, 3, 5$. Subfigures (a) - (c) display $l = 2$, while Subfigures (d) - (e) correspond to $l = 3$.

$$\begin{aligned}
 I_z(\Delta m, M) &\equiv \int_0^h dz z \sin\left(\frac{m\pi}{h}z\right) \sin\left(\frac{m'\pi}{h}z\right) \\
 &= \begin{cases} 0 & \text{if } \Delta m \neq 0 \text{ and } M \neq 0 \text{ are even integers.} \\ 4h^2/\pi^2 (1/\Delta m^2 - 1/M^2) & \text{If } \Delta m \neq 0 \text{ and } M \neq 0 \text{ are odd integers} \\ h^2/4 & \text{if } \Delta m = 0 \text{ and } M \neq 0 \text{ (even)} \\ -h^2/4 & \text{if } M = 0 \text{ and } \Delta m \neq 0 \text{ (even)} \end{cases}, \quad (26)
 \end{aligned}$$

enforces a few basic selection rules. Moreover, we notice that in order to have a non-vanishing integral, Δm and M must have the same parity.

As a specific numerical example, the following matrix gives

the values of the first 64 elements of the transition $|T_z|$ between $|111; 1^+\rangle \rightarrow |nm1, 1^+\rangle$ for a TI-NP made of Bi_2Te_3 with $R = 10R_0$, $h = R_0$, and $\alpha = \pi/6$:

$$\begin{pmatrix} 8 & 2.88091 & 0 & 0.23035 & 0 & 0.0634495 & 0 & 0.0261078 \\ 7.33474 & 2.64153 & 0 & 0.211215 & 0 & 0.0581791 & 0 & 0.0239392 \\ 0 & 0 & 0 & 0 & 0 & 0 & 0 & 0 \\ 1.96007 & 0.706002 & 0 & 0.0564561 & 0 & 0.015551 & 0 & 0.00639883 \\ 0 & 0 & 0 & 0 & 0 & 0 & 0 & 0 \\ 1.24078 & 0.446931 & 0 & 0.0357421 & 0 & 0.00984537 & 0 & 0.00405114 \\ 0 & 0 & 0 & 0 & 0 & 0 & 0 & 0 \\ 0.936291 & 0.337241 & 0 & 0.026972 & 0 & 0.00742969 & 0 & 0.00305715 \end{pmatrix} \quad (27)$$

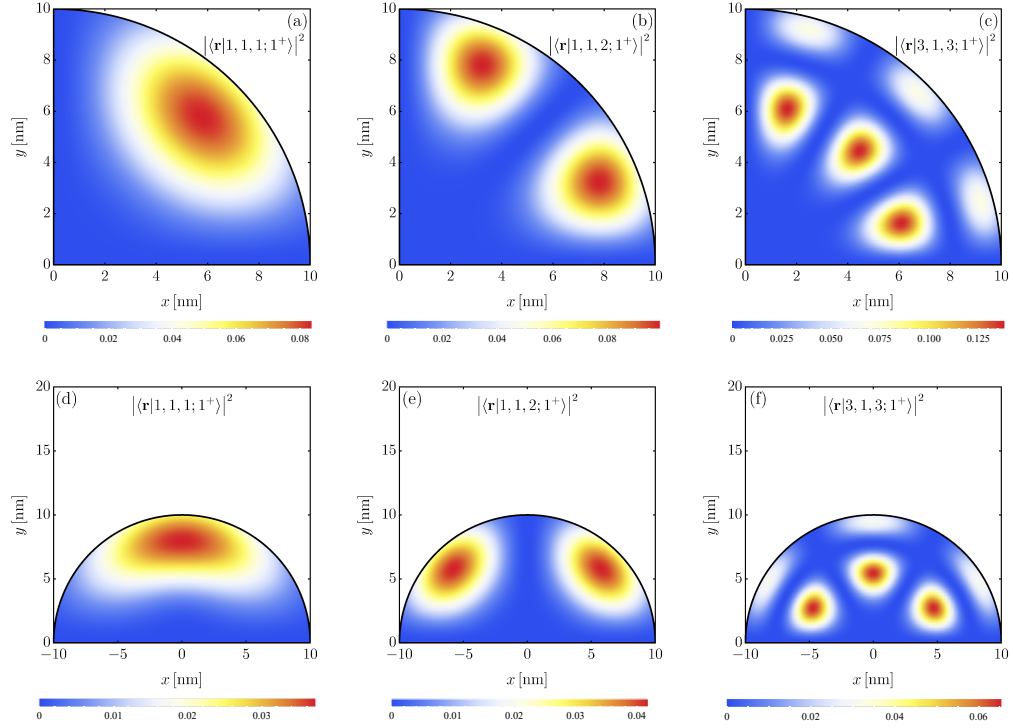


FIG. 7: Probability density for $\alpha = \pi/2$ and $\alpha = \pi$ in $z = 0.5h$, for different values of n and l , and fixed m .

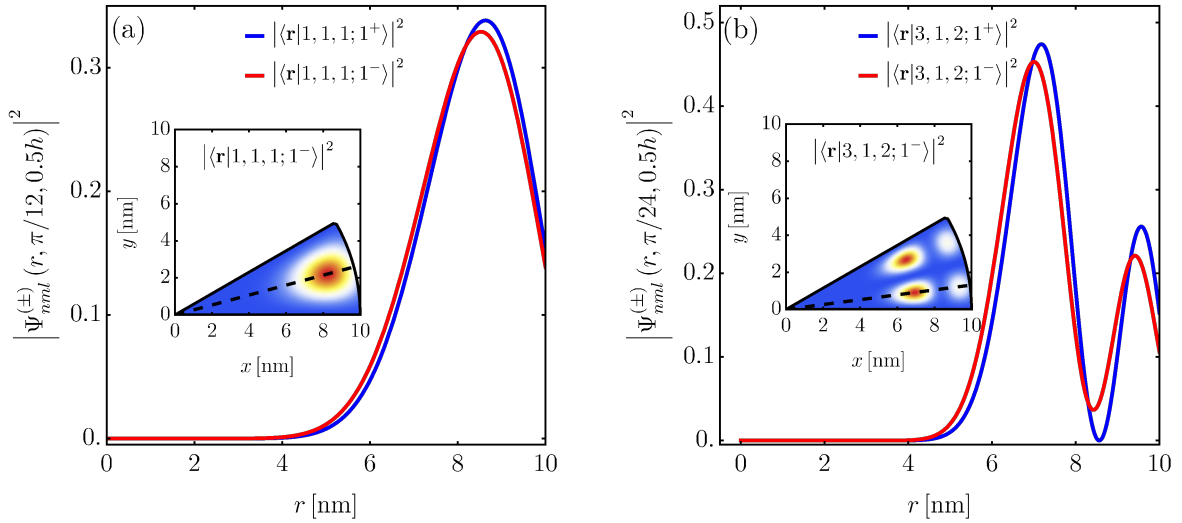


FIG. 8: Comparison between the probability density distribution for the states $|nml; 1^+\rangle$ and $|nml; 1^-\rangle$ as a function of the radial coordinate. The insets show the 2D probability density at $z = 0.5h$ and the dashed line is the direction where the main plot is constructed.

Analogous analytical expressions are obtained for the following transition amplitudes:

$$\begin{aligned}
T_z(|2^\pm\rangle \rightarrow |2^\pm\rangle) &= \frac{e\alpha}{2} B_\pm B'_\pm \delta_{ll'} \left\{ \kappa \kappa' (\mathcal{M} \pm \widetilde{\mathcal{M}}) (\mathcal{M}' \pm \widetilde{\mathcal{M}}') \widetilde{I}_n^{n'} I_z(\Delta m, M) \right. \\
&\quad + \left[k k' (\mathcal{M} \pm \widetilde{\mathcal{M}}) (\mathcal{M}' \pm \widetilde{\mathcal{M}}') + 1 \right] I_n^{n'} I_z(\Delta m, M) \\
&\quad \left. + \frac{i\hbar R_0}{4} \delta_{mm'} \left[k (\mathcal{M} \pm \widetilde{\mathcal{M}}) - k' (\mathcal{M}' \pm \widetilde{\mathcal{M}}') \right] I_n^{n'} \right\}, \tag{28}
\end{aligned}$$

$$\begin{aligned}
T_z(|1^\pm\rangle \rightarrow |1^\mp\rangle) &= \frac{e\alpha}{2} A_\pm A'_\mp \delta_{ll'} \left\{ \kappa \kappa' (-\mathcal{M} \pm \widetilde{\mathcal{M}}) (-\mathcal{M}' \mp \widetilde{\mathcal{M}}') I_n^{n'} I_z(\Delta m, M) \right. \\
&\quad + \left[k k' (-\mathcal{M} \pm \widetilde{\mathcal{M}}) (-\mathcal{M}' \mp \widetilde{\mathcal{M}}') + 1 \right] \widetilde{I}_n^{n'} I_z(\Delta m, M) \\
&\quad \left. + \frac{i\hbar R_0}{4} \delta_{mm'} \left[k' (-\mathcal{M}' \mp \widetilde{\mathcal{M}}') - k (-\mathcal{M} \pm \widetilde{\mathcal{M}}) \right] \widetilde{I}_n^{n'} \right\}, \tag{29}
\end{aligned}$$

$$\begin{aligned}
T_z(|2^\pm\rangle \rightarrow |2^\mp\rangle) &= \frac{e\alpha}{2} B_\pm B'_\mp \delta_{ll'} \left\{ \kappa \kappa' (\mathcal{M} \pm \widetilde{\mathcal{M}}) (\mathcal{M}' \mp \widetilde{\mathcal{M}}') \widetilde{I}_n^{n'} I_z(\Delta m, M) \right. \\
&\quad + \left[k k' (\mathcal{M} \pm \widetilde{\mathcal{M}}) (\mathcal{M}' \mp \widetilde{\mathcal{M}}') + 1 \right] I_n^{n'} I_z(\Delta m, M) \\
&\quad \left. + \frac{i\hbar R_0}{4} \delta_{mm'} \left[k (\mathcal{M} \pm \widetilde{\mathcal{M}}) - k' (\mathcal{M}' \mp \widetilde{\mathcal{M}}') \right] I_n^{n'} \right\}, \tag{30}
\end{aligned}$$

$$\begin{aligned}
T_z(|1^\pm\rangle \rightarrow |2^\pm\rangle) &= \frac{e\alpha}{2} A_\pm B'_\pm \delta_{ll'} \left\{ i (\mathcal{M}' \pm \widetilde{\mathcal{M}}') (-\mathcal{M} \pm \widetilde{\mathcal{M}}) \left[k' \kappa I_n^{n'} - k \kappa' \widetilde{I}_n^{n'} \right] I_z(\Delta m, M) \right. \\
&\quad \left. + \frac{\hbar R_0}{4} \delta_{mm'} \left[\kappa' (\mathcal{M}' \pm \widetilde{\mathcal{M}}') \widetilde{I}_n^{n'} - \kappa (-\mathcal{M} \pm \widetilde{\mathcal{M}}) I_n^{n'} \right] \right\}, \tag{31}
\end{aligned}$$

and

$$\begin{aligned}
T_z(|1^\pm\rangle \rightarrow |2^\mp\rangle) &= \frac{e\alpha}{2} A_\pm B'_\pm \delta_{ll'} \left\{ i (\mathcal{M}' \mp \widetilde{\mathcal{M}}') (-\mathcal{M} \pm \widetilde{\mathcal{M}}) \left[k' \kappa I_n^{n'} - k \kappa' \widetilde{I}_n^{n'} \right] I_z(\Delta m, M) \right. \\
&\quad \left. + \frac{\hbar R_0}{4} \delta_{mm'} \left[\kappa' (\mathcal{M}' \mp \widetilde{\mathcal{M}}') \widetilde{I}_n^{n'} - \kappa (-\mathcal{M} \pm \widetilde{\mathcal{M}}) I_n^{n'} \right] \right\}. \tag{32}
\end{aligned}$$

Figure 9 shows the selection rules in Bi_2Se_3 for the transition $|1, 1, 1; 1^+\rangle \rightarrow |n, 1, 1; 1^+\rangle$ (Fig. 9-(a)), and $|1, 1, 1; 1^+\rangle \rightarrow |n, 1, 1; 2^+\rangle$ (Fig. 9-(b)) and as a function of n and the ratio h/R_0 for $\alpha = \pi/6$ and $R = R_0$, respectively. In addition to the conditions stated in Eq. (26) and $l = l'$, it is clear that transitions with Δn even are forbidden. Moreover, we find that the amplitude of the matrix elements for T_z increases proportionally to h/R_0 for $|1, 1, 1; 1^+\rangle \rightarrow |n, 1, 1; 1^+\rangle$, as can be noticed in the inset of Fig. 9-(a). This finite-size effect is related to the delocalization of the particle in the z -direction. In fact, the element $|1, 1, 1; 1^+\rangle \rightarrow |1, 1, 1; 1^+\rangle$ can be interpreted as a polariza-

tion of the electronic wave function, which spreads over all the region when $h \rightarrow \infty$ (it turns to be a plane wave $e^{\pm ikz}$ where the dipole approximation is not longer valid). On the other hand, the case $|1, 1, 1; 1^+\rangle \rightarrow |n, 1, 1; 2^+\rangle$ presents a saturation value displayed by the yellow line in Fig. 9-(b). Finally, our numerical calculations demonstrate that for these transition amplitudes the values of R and α do not provide an appreciable change in the profiles of Fig. 9.

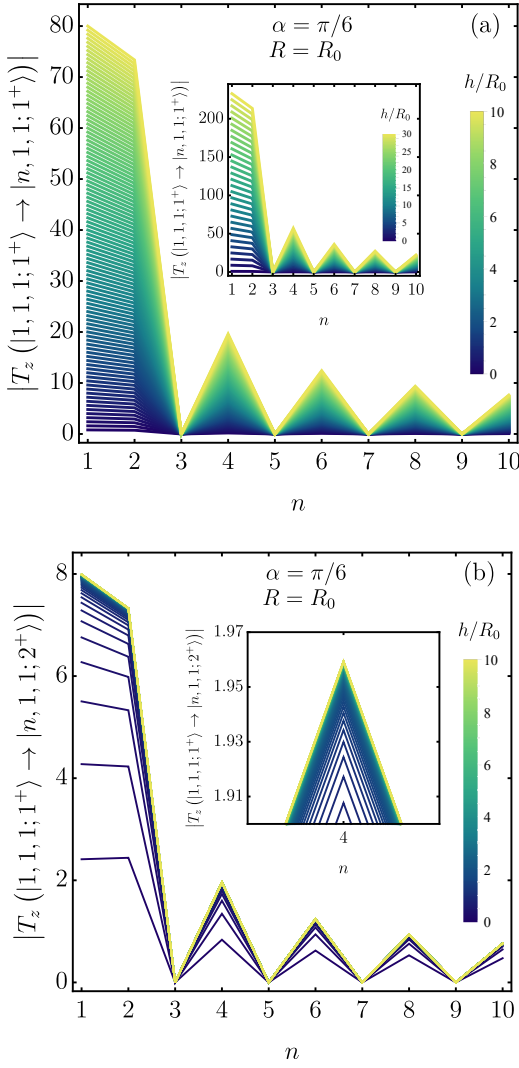


FIG. 9: Selection rule in z -direction for a TI nanoparticle made of Bi_2Se_3 with a radius $R = R_0$ and $\alpha = \pi/6$. The figure shows the allowed and forbidden transitions from the ground state as a function of the height h .

B. Transition amplitudes in $x \pm iy$ -direction

Let us now consider the transition amplitudes in the $x \pm iy$ -direction, given by the analytical expression

$$\begin{aligned}
 T_{x \pm iy}(|1^\pm\rangle \rightarrow |1^\pm\rangle) &= \frac{eh}{2} A_\pm A'_\pm \delta_{mm'} \\
 &\times \left\{ \kappa \kappa' \left(-\mathcal{M} \pm \widetilde{\mathcal{M}} \right) \left(-\mathcal{M}' \pm \widetilde{\mathcal{M}}' \right) I_\phi^\pm(\Delta l, L) J_{nl}^{n'l'} \right. \\
 &+ \left[k k' \left(-\mathcal{M} \pm \widetilde{\mathcal{M}} \right) \left(-\mathcal{M}' \pm \widetilde{\mathcal{M}}' \right) + 1 \right] I_\phi^\pm(\Delta l, L) \widetilde{J}_{nl}^{n'l'} \\
 &\left. - i R_0 \kappa' \left(-\mathcal{M}' \pm \widetilde{\mathcal{M}}' \right) I_\phi^+(\Delta l, L) \widetilde{K}_{nl}^{n'l'} \right\}, \quad (33)
 \end{aligned}$$

where the coefficients $J_{nl}^{n'l'}$, $\widetilde{J}_{nl}^{n'l'}$ and $\widetilde{K}_{nl}^{n'l'}$ are defined in Sec. 3 of the Supplemental. On the other hand, for $\Delta l = l' - l$

and $L = l + l'$, the coefficients $I_\phi^\pm(\Delta l, L)$ are defined by the expression

$$\begin{aligned}
 I_\phi^\pm(\Delta l, L) &\equiv \int_0^\alpha d\phi e^{\pm i\phi} \sin\left(\frac{l\pi}{\alpha}\phi\right) \sin\left(\frac{l'\pi}{\alpha}\phi\right) \\
 &= \frac{\alpha}{2} \frac{e^{\pm i\alpha} [\pi \Delta l \sin(\pi \Delta l) \pm i\alpha \cos(\pi \Delta l)] \mp i\alpha}{(\pi^2 \Delta l^2 - \alpha^2)} \\
 &- \frac{\alpha}{2} \frac{e^{\pm i\alpha} [\pi L \sin(\pi L) \pm i\alpha \cos(\pi L)] \mp i\alpha}{(\pi^2 L^2 - \alpha^2)}. \quad (34)
 \end{aligned}$$

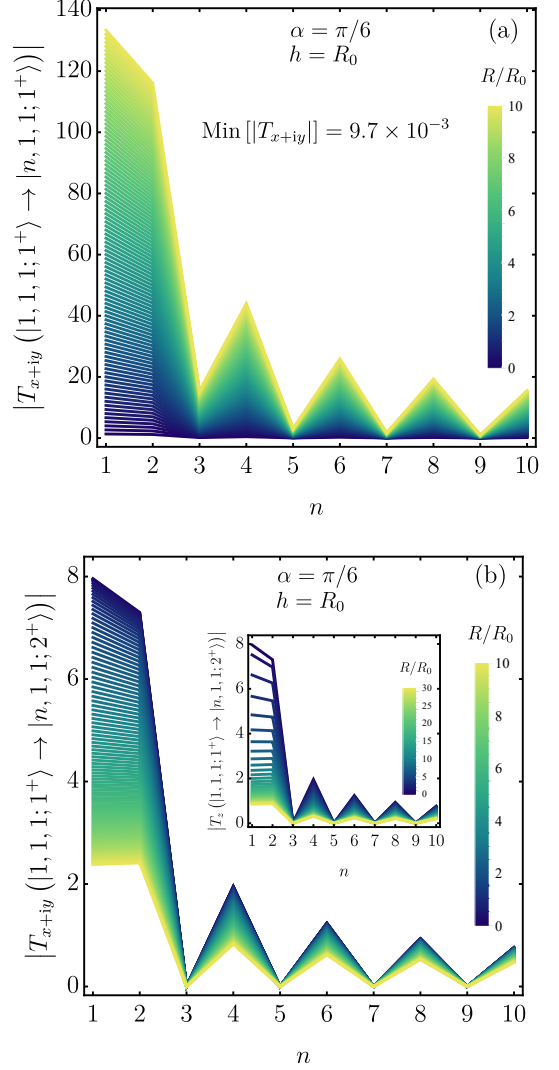


FIG. 10: Selection rule in $x + iy$ -direction for a TI nanoparticle made of Bi_2Se_3 with a height $h = R_0$ and $\alpha = \pi/6$. The figure shows the allowed and forbidden transitions from the ground state as a function of the radius R .

The selection rules in the $x + iy$ -direction are understood from the information presented in Figs. 10 and 11. In this case, the relevant confinement parameter is R , so that variations on h and α produce only tiny effects. Also, the transition $|1, 1, 1, 1^+\rangle \rightarrow |n, 1, 1, 1^+\rangle$ is enhanced as R grows, while the

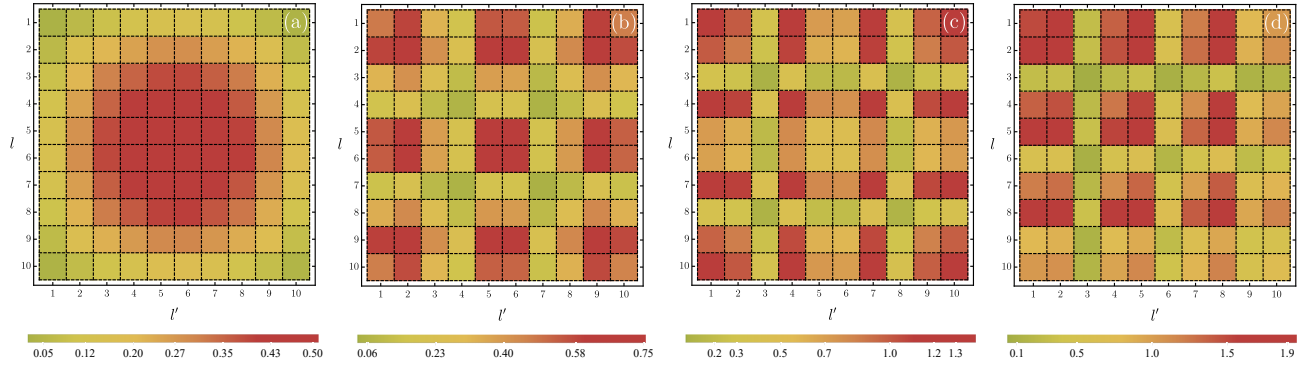


FIG. 11: Tomography of the integral $|I_\phi^+|$ defined in Eq. (34) as a function of the angular quantum number for the initial (l) and final (l') states. Panel (a) is the case for $\alpha = \pi/6$, panel (b) for $\alpha = \pi/4$, (c) for $\alpha = \pi/2$, and (d) for $\alpha = \pi$.

transition $|1, 1, 1; 1^+\rangle \rightarrow |n, 1, 1; 2^+\rangle$ is reduced. Moreover, in Fig. 10(a) the amplitude of the matrix element $|T_{x+iy}|$ is never zero, being 9.7×10^{-3} its minimum value in the range plotted. Therefore, strictly speaking there is not a selection rule for n but the transition is highly suppressed for $n > 3$.

In contrast with the former, Fig. 10(b) shows the existence of a selection rule for $|1, 1, 1; 1^+\rangle \rightarrow |n, 1, 1; 2^+\rangle$ so that the transition is only allowed for Δn odd. Finally, from the mathematical expressions, it is clear that the transition is allowed for $\Delta m = 0$, and as Fig. 11 suggests there are no restrictions over Δl .

Transition	Δn	Δm	Δl
$T_z(1, 1, 1; 1^+\rangle \rightarrow n, m, l; 1^+\rangle)$ $T_z(1, 1, 1; 1^+\rangle \rightarrow n, m, l; 1^-\rangle)$ $T_z(1, 1, 1; 1^+\rangle \rightarrow n, m, l; 2^+\rangle)$ $T_z(1, 1, 1; 1^+\rangle \rightarrow n, m, l; 2^-\rangle)$ $T_z(1, 1, 1; 2^+\rangle \rightarrow n, m, l; 2^+\rangle)$ $T_z(1, 1, 1; 2^+\rangle \rightarrow n, m, l; 2^-\rangle)$	Odd	Given by Eq. (26)	0
$T_{x+iy}(1, 1, 1; 1^+\rangle \rightarrow n, m, l; 1^+\rangle)$ $T_{x+iy}(1, 1, 1; 1^+\rangle \rightarrow n, m, l; 1^-\rangle)$	No restrictions (highly suppressed for $n > 3$)		
$T_{x+iy}(1, 1, 1; 1^+\rangle \rightarrow n, m, l; 2^+\rangle)$ $T_{x+iy}(1, 1, 1; 1^+\rangle \rightarrow n, m, l; 2^-\rangle)$ $T_{x+iy}(1, 1, 1; 2^+\rangle \rightarrow n, m, l; 2^+\rangle)$ $T_{x+iy}(1, 1, 1; 2^+\rangle \rightarrow n, m, l; 2^-\rangle)$	Odd	0	No restrictions

TABLE II: Selection rules for the transitions $T_\mu(|1, 1, 1; q^s\rangle \rightarrow |n, m, l; q^{s'}\rangle)$ with $n > 1$. The values of R , h , and α are arbitrary.

V. CONCLUSIONS

In this article, we studied the effects of size and morphology on the confined electronic states in TI-NPs, including the transition amplitudes and selection rules for transitions within the dipole approximation. Moreover, by means of a spatial representation of the probability density distribution, we identified the conditions leading to the emergence of topologically trivial surface states arising from the underlying bulk band structure. The existence of such surface states is predicted in our theoretical formulation of the problem, since we incorporated a more general boundary condition involving the vanishing of the normal component of the probability current at

the boundary [41–44], in contrast with the hard-wall applied in previous studies reported in the literature [37, 47], where the full eigenstate vanishes at the boundary by construction. The predicted existence of these topologically trivial surface states arising from the bulk upon geometric confinement, supports the idea that they might couple and interact with the topologically protected surface states in TI nanostructures, as suggested by magnetotransport experiments [20, 21, 28–33]. The nature of the coupling mechanism, that in addition to confinement might involve disorder and many-body effects [20, 21, 28, 30, 31, 34], is a subject of further study that goes beyond the scope of the present work.

ACKNOWLEDGEMENTS

J.D.C.-Y. and E.M. acknowledge financial support from ANID PIA Anillo ACT/192023. E.M. also acknowledges financial support from Fondecyt 1190361.

AUTHOR CONTRIBUTIONS STATEMENT

E.M. conceived the study and supervised the work. J.D.C.-Y. and E.M. performed the analytical calculations. J.D.C.-Y. performed numerical calculations to generate all the figures. All authors reviewed the manuscript.

-
- [1] Ching-Kai Chiu, Jeffrey C. Y. Teo, Andreas P. Schnyder, and Shinsei Ryu, "Classification of topological quantum matter with symmetries," *Rev. Mod. Phys.* **88**, 035005 (2016).
- [2] M. Z. Hasan and C. L. Kane, "Colloquium: Topological insulators," *Rev. Mod. Phys.* **82**, 3045–3067 (2010).
- [3] Xiao-Liang Qi and Shou-Cheng Zhang, "Topological insulators and superconductors," *Rev. Mod. Phys.* **83**, 1057–1110 (2011).
- [4] Pedram Roushan, Jungpil Seo, Colin V. Parker, Y. S. Hor, D. Hsieh, Dong Qian, Anthony Richardella, M. Z. Hasan, R. J. Cava, and Ali Yazdani, "Topological surface states protected from backscattering by chiral spin texture," *Nature* **460**, 1106–1109 (2009).
- [5] Ning Xu, Yong Xu, and Jia Zhu, "Topological insulators for thermoelectrics," *npj Quantum Materials* **2**, 51 (2017).
- [6] B. A. Bernevig, T. L. Hughes, and S.-C. Zhang, "Quantum Spin Hall Effect and topological phase transition in *hgte* quantum wells," *Science* **314**, 1757–1761 (2006).
- [7] M. König, S. Wiedmann, C. Brüne, A. Roth, H. Buhmann, L. W. Molenkamp, X. L. Qi, and S.-C. Zhang, "Quantum Spin Hall insulator state in HgTe quantum wells," *Science* **318**, 766–770 (2006).
- [8] L. Fu, C. L. Kane, and E. J. Mele, "Topological insulators in three dimensions," *Phys. Rev. Lett.* **98**, 106803 (2007).
- [9] D. Hsieh, D. Qian, L. Wray, Y. Xia, Y. S. Hor, R. J. Cava, and M. Z. Hasan, "A topological Dirac insulator in a quantum spin Hall phase," *Nature* **452**, 970–974 (2008).
- [10] Y. Xia, D. Qian, D. Hsieh, L. Wray, A. Pal, H. Lin, A. Bansil, D. Grauer, Y. S. Hor, R. J. Cava, and M. Z. Hasan, "Observation of a large-gap topological-insulator class with a single Dirac cone on the surface," *Nature Phys.* **5**, 398–402 (2009).
- [11] H. Zhang, C.-X. Liu, X.-L. Qi, X. Dai, Z. Fang, and S.-C. Zhang, "Topological insulators in Bi_2Se_3 , Bi_2Te_3 and Sb_2Te_3 with a single Dirac cone on the surface," *Nature Physics* **5**, 438 (2009).
- [12] A. K. Geim and I. V. Grigorieva, "Van der waals heterostructures," *Nature* **499**, 419–425 (2013).
- [13] H. Peng, K. Lai, D. Kong, S. Meister, Y. Chen, X.-L. Qi, S.-C. Zhang, Z.-X. Shen, and Y. Cui, "Aharonov–bohm interference in topological insulator nanoribbons," *Nature Mater.* **9**, 225–229 (2010).
- [14] D. Kong, J. C. Randel, H. Peng, J. J. Cha, S. Meister, K. Lai, Y. Chen, Z.-X. Shen, H. C. Manoharan, and Y. Cui, "Topological insulator nanowires and nanoribbons," *Nano Lett.* **10**, 329–333 (2010).
- [15] D. Kong, W. Dang, J. J. Cha, H. Li, S. Meister, H. Peng, Z. Liu, and Y. Cui, "Few-layer nanoplates of Bi_2Se_3 and Bi_2Te_3 with highly tunable chemical potential," *Nano Lett.* **10**, 2245–2250 (2010).
- [16] Pascal Gehring, Bo F. Gao, Marko Burghard, and Klaus Kern, "Growth of high-mobility $\text{Bi}_2\text{Te}_2\text{Se}$ nanoplatelets on hBN sheets by van der Waals epitaxy," *Nano Letters* **12**, 5137–5142 (2012), pMID: 22985022, <https://doi.org/10.1021/nl3019802>.
- [17] Desheng Kong, Kristie J. Koski, Judy J. Cha, Seung Sae Hong, and Yi Cui, "Ambipolar Field Effect in Sb-Doped Bi_2Se_3 Nanoplates by Solvothermal Synthesis," *Nano Letters* **13**, 632–636 (2013), pMID: 23323715, <https://doi.org/10.1021/nl304212u>.
- [18] Faxian Xiu, Liang He, Yong Wang, Lina Cheng, Li-Te Chang, Murong Lang, Guan Huang, Xufeng Kou, Yi Zhou, Xiaowei Jiang, Zhigang Chen, Jin Zou, Alexandros Shailos, and Kang L. Wang, "Manipulating surface states in topological insulator nanoribbons," *Nature Nanotechnology* **6**, 216–221 (2011).
- [19] A. Purkayastha, F. Lupo, S. Kim, T. Borca-Tasciuc, and G. Ramanath, "Low-temperature, template-free synthesis of single-crystal bismuth telluride nanorods," *Advanced Materials* **18**, 496–500 (2006).
- [20] J. G. Checkelsky, Y. S. Hor, R. J. Cava, and N. P. Ong, "Bulk band gap and surface state conduction observed in voltage-tuned crystals of the topological insulator bi_2se_3 ," *Phys. Rev. Lett.* **106**, 196801 (2011).
- [21] Dohun Kim, Sungjae Cho, Nicholas P. Butch, Paul Syers, Kevin Kirshenbaum, Shaffique Adam, Johnpierre Paglione, and Michael S. Fuhrer, "Surface conduction of topological dirac electrons in bulk insulating bi_2se_3 ," *Nature Physics* **8**, 459–463 (2012).
- [22] Seung Sae Hong, Worasom Kundhikanjana, Judy J. Cha, Keji Lai, Desheng Kong, Stefan Meister, Michael A. Kelly, Zhi-Xun Shen, and Yi Cui, "Ultrathin topological insulator bi_2se_3 nanoribbons exfoliated by atomic force microscopy," *Nano Letters* **10**, 3118–3122 (2010), pMID: 20698625, <https://doi.org/10.1021/nl101884h>.
- [23] Valeria Nicolosi, Manish Chhowalla, Mercouri G. Kanatzidis, Michael S. Strano, and Jonathan N. Coleman, "Liquid exfoliation of layered materials," *Science* **340**, 1226419 (2013), <https://www.science.org/doi/pdf/10.1126/science.1226419>.
- [24] C. Parra, T. Rodrigues da Cunha, A. W. Contryman, D. Kong, F. Montero-Silva, P. H. Rezende Goncalves, D. Duarte Dos Reis, P. Giraldo-Gallo, R. Segura, F. Olivares, F. Niemetski, Y. Cui, R. Magalhaes-Paniago, and H. Manoharan, "Phase Separation of Dirac Electrons in Topological Insulators at the Spatial Limit," *Nano Lett.* **17**, 97–103 (2017).
- [25] P. H. R. Goncalves, T. Chagas, V. B. Nascimento, dos Reis, D. D., C. Parra, M. S. C. Mazzoni, A. Malachias, and R. Magalhaes-Paniago, "Formation of Bi_xSe_y Phases Upon Annealing of the Topological Insulator Bi_2Se_3 : Stabilization of In-Depth Bismuth Bilayers," *J. Phys. Chem. Lett.* **9**, 954–960 (2018).
- [26] J. Fang, Y. Jia, D. J. Miller, M. L. Latimer, Z. L. Xiao, U. Welp, G. W. Crabtree, and W.-K. Kwok, "Catalyst-Free Growth of Millimeter-Long Topological Insulator Bi_2Se_3 Nanoribbons and the Observation of the π -Berry Phase," *Nano Lett.* **12**, 6164–6169 (2012).
- [27] Y.-C. Zou, Z.-G. Chen, E. Zhang, F. Kong, Y. Lu, L. Wang, J. Drennan, Z. Wang, F. Xiu, K. Cho, and J. Zou, "Atomic

- disorders in layer structured topological insulator $SnBi_2Te_4$ nanoplates,” *Nano Res.* **11**, 696–706 (2019).
- [28] Olivio Chiatti, Christian Riha, Dominic Lawrenz, Marco Busch, Srujana Dusari, Jaime Sánchez-Barriga, Anna Mogilatenko, Lada V. Yashina, Sergio Valencia, Akin A. Ünal, Oliver Rader, and Saskia F. Fischer, “2d layered transport properties from topological insulator Bi_2Se_3 single crystals and micro flakes,” *Scientific Reports* **6**, 27483 (2016).
- [29] Hao Tang, Xuejun Yan, Yucheng Xiong, Kunpeng Dou, Yang Zhao, Jiansheng Jie, Xiaomeng Wang, Qiang Fu, Juekuan Yang, Minghui Lu, and Dongyan Xu, “Quantum transport characteristics of heavily doped bismuth selenide nanoribbons,” *npj Quantum Materials* **4**, 1 (2019).
- [30] Jian Liao, Yunbo Ou, Haiwen Liu, Ke He, Xucun Ma, Qi-Kun Xue, and Yongqing Li, “Enhanced electron dephasing in three-dimensional topological insulators,” *Nature Communications* **8**, 16071 (2017).
- [31] Mingliang Tian, Wei Ning, Zhe Qu, Haifeng Du, Jian Wang, and Yuheng Zhang, “Dual evidence of surface dirac states in thin cylindrical topological insulator Bi_2Te_3 nanowires,” *Scientific Reports* **3**, 1212 (2013).
- [32] H. Steinberg, J.-B. Laloë, V. Fatemi, J. S. Moodera, and P. Jarillo-Herrero, “Electrically tunable surface-to-bulk coherent coupling in topological insulator thin films,” *Phys. Rev. B* **84**, 233101 (2011).
- [33] Yanfei Zhao, Cui-Zu Chang, Ying Jiang, Ashley DaSilva, Yi Sun, Huichao Wang, Ying Xing, Yong Wang, Ke He, Xucun Ma, Qi-Kun Xue, and Jian Wang, “Demonstration of surface transport in a hybrid Bi_2Se_3/Bi_2Te_3 heterostructure,” *Scientific Reports* **3**, 3060 (2013).
- [34] Hai-Zhou Lu and Shun-Qing Shen, “Weak localization of bulk channels in topological insulator thin films,” *Phys. Rev. B* **84**, 125138 (2011).
- [35] Chao-Xing Liu, Xiao-Liang Qi, HaiJun Zhang, Xi Dai, Zhong Fang, and Shou-Cheng Zhang, “Model hamiltonian for topological insulators,” *Phys. Rev. B* **82**, 045122 (2010).
- [36] K.-I. Imura, Y. Yoshimura, Y. Takane, and T. Fukui, “Spherical topological insulator,” *Phys. Rev. B* **86**, 235119 (2012).
- [37] M. Governale, B. Bhandari, F. Taddei, K.-I. Imura, and U. Zülicke, “Finite-size effects in cylindrical topological insulators,” *New J. Phys.* **22**, 063042 (2020).
- [38] Jorge David Castano-Yepes, DA Amor-Quiroz, CF Ramirez-Gutierrez, and Edgar A Gómez, “Impact of a topological defect and Rashba spin-orbit interaction on the thermo-magnetic and optical properties of a 2D semiconductor quantum dot with Gaussian confinement,” *Physica E* **109**, 59–66 (2019).
- [39] Jorge David Castaño-Yepes, O.J. Franca, C.F. Ramirez-Gutierrez, and J.C. del Valle, “Optical intersubband properties of a core-shell semiconductor-topological insulator quantum dot described by θ -electrodynamics,” *Physica E* **123**, 114202 (2020).
- [40] Bernd Thaller, *The Dirac equation* (Springer Science & Business Media, 2013).
- [41] K. Johnson, “The M.I.T bag model,” *Acta Phys. Pol. B* **6**, 865–892 (1975).
- [42] A. Chodos, R. L. Jaffe, K. Johnson, C. B. Thorn, and V. F. Weisskopf, “New extended model of hadrons,” *Phys. Rev. D* **9**, 3471–3495 (1974).
- [43] A. Chodos, R. L. Jaffe, K. Johnson, and C. B. Thorn, “Baryon structure in the bag theory,” *Phys. Rev. D* **10**, 2599–2604 (1974).
- [44] A. Chodos, “Field-theoretic lagrangian with baglike solutions*,” *Phys. Rev. D* **12**, 2397–2406 (1975).
- [45] I. A. Nechaev and E. E. Krasovskii, “Relativistic $\mathbf{k} \cdot \mathbf{p}$ Hamiltonians for centrosymmetric topological insulators from ab initio wave functions,” *Phys. Rev. B* **94**, 201410(R) (2016).
- [46] B. A. Assaf, T. Phuphachong, V. V. Volobuev, G. Bauer, B. Springholz, L.-A. Vaulchier, and Y. Guldner, “Magneto-optical determination of a topological index,” *npj Quantum Materials* **2**, 26 (2017).
- [47] L. Gioia, M. G. Christie, U. Zülicke, M. Governale, and A. J. Sneyd, “Spherical topological insulator nanoparticles: Quantum size effects and optical transitions,” *Phys. Rev. B* **100**, 205417 (2019).

Supplemental Material for "The role of morphology on the emergence of topologically trivial surface states and selection rules in topological-insulator nanoparticles"

Jorge David Castaño-Yepes^{1,*} and Enrique Muñoz^{1,2,†}

¹Physics Institute, Pontificia Universidad Católica de Chile, Vicuña Mackenna 4860, Santiago, Chile.

²Research Center for Nanotechnology and Advanced-Materials CIEN-UC, Pontificia Universidad Católica de Chile, Vicuña Mackenna 4860, Santiago, Chile.

In this Supplemental material, we present the details of the mathematical analysis leading to the solution of the confined spinor eigenstates in a TI nanoparticle (TI-NP). The text is organized in four separate sections. In the first one, we obtain the correct analytical expression for the probability current, by deriving the exact form of the continuity equation corresponding to the Hamiltonian of the model. In the second section, we derive the rigorous mathematical solution to the eigenvalue problem for the bulk Hamiltonian operator in the Dirac limit, i.e. when the mass operator reduces to a constant $\mathbb{M}(\mathbf{k}^2) \rightarrow \Delta_0$. Based on the spinor structure of the explicit solutions for this case, we derive in the third section the analytical solution for the corresponding eigenstates of the problem involving the full mass operator $\mathbb{M}(\mathbf{k}^2)$. Finally, in the fourth section we present the explicit calculation of the transition amplitudes, and the corresponding selection rules, within the electric dipole approximation, as predicted from the explicit spinor eigenstates obtained in section 3.

I. THE BULK HAMILTONIAN AND THE PROBABILITY CURRENT

In the main text, we defined the mass operator

$$\mathbb{M}(\mathbf{k}) \equiv \frac{\Delta_0}{2} + \frac{\gamma}{k_\Delta} \mathbf{k}^2, \quad (1)$$

so that the bulk Hamiltonian reads

$$\hat{\mathcal{H}} = \mathbb{M}(\mathbf{k})\hat{\beta} + \gamma(\boldsymbol{\alpha} \cdot \mathbf{k}), \quad (2)$$

where we defined the Dirac 4×4 matrices in the standard representation

$$\boldsymbol{\alpha} = \begin{pmatrix} 0 & \boldsymbol{\sigma} \\ \boldsymbol{\sigma} & 0 \end{pmatrix}, \quad \hat{\beta} = \begin{pmatrix} \mathbb{1} & 0 \\ 0 & -\mathbb{1} \end{pmatrix}. \quad (3)$$

To derive the analytical expression for the current density \mathbf{J} , we start by defining the normalized probability density $\rho(\mathbf{r}, t) = \Psi^\dagger(\mathbf{r}, t)\Psi(\mathbf{r}, t)$ in the region Ω representing the TI-NP,

$$\int_{\Omega} d^3x \rho(\mathbf{r}, t) = \int_{\Omega} d^3x \Psi^\dagger(\mathbf{r}, t)\Psi(\mathbf{r}, t) = 1, \quad (4)$$

with $\Psi(\mathbf{r}, t)$ the spinor states satisfying the time evolution equation

$$\partial_t \Psi = -i\hat{\mathcal{H}}\Psi. \quad (5)$$

Therefore, taking the time derivative of Eq. (4), we obtain

$$\partial_t \left(\int_{\Omega} d^3x \rho(\mathbf{r}, t) \right) = \int_{\Omega} d^3x [(\partial_t \Psi^\dagger) \Psi + \Psi^\dagger (\partial_t \Psi)] = 0. \quad (6)$$

Now, from the time-evolution Eq. (5) and its hermitian conjugate, we have

$$\int_{\Omega} d^3x \partial_t \rho(\mathbf{r}, t) = \int_{\Omega} d^3x \left[i \left(\hat{\mathcal{H}}\Psi \right)^\dagger \Psi - i \Psi^\dagger \left(\hat{\mathcal{H}}\Psi \right) \right] = 0. \quad (7)$$

* jcastano@fis.uc.cl

† munozt@fis.puc.cl

Given that the Hamiltonian is hermitian, $\hat{\mathcal{H}} = \hat{\mathcal{H}}^\dagger$, the above expression reduces to

$$\begin{aligned} \int_{\Omega} d^3x \partial_t \rho(\mathbf{r}, t) &= \int_{\Omega} d^3x \left[i \left(\frac{\Delta_0}{2} - \frac{\gamma}{k_{\Delta}} \nabla^2 \right) \Psi^\dagger (\tau_z \otimes \sigma_0) \Psi - i \Psi^\dagger (\tau_z \otimes \sigma_0) \left(\frac{\Delta_0}{2} - \frac{\gamma}{k_{\Delta}} \nabla^2 \right) \Psi \right] \\ &\quad - \int_{\Omega} d^3x [(\nabla \Psi^\dagger \cdot \boldsymbol{\alpha}) + \Psi^\dagger \boldsymbol{\alpha} \cdot (\nabla \Psi)], \end{aligned} \quad (8)$$

therefore,

$$\begin{aligned} \int_{\Omega} d^3x \partial_t \rho(\mathbf{r}, t) &= -i \frac{\gamma}{k_{\Delta}} \int_{\Omega} d^3x [\nabla^2 \Psi^\dagger (\tau_z \otimes \sigma_0) \Psi - \Psi^\dagger (\tau_z \otimes \sigma_0) \nabla^2 \Psi] - \int_{\Omega} d^3x [(\nabla \Psi^\dagger \cdot \boldsymbol{\alpha}) + \Psi^\dagger \boldsymbol{\alpha} \cdot (\nabla \Psi)] \\ &= -i \frac{\gamma}{k_{\Delta}} \int_{\Omega} d^3x \nabla \cdot [\nabla \Psi^\dagger (\tau_z \otimes \sigma_0) \Psi - \Psi^\dagger (\tau_z \otimes \sigma_0) \nabla \Psi] - \int_{\Omega} d^3x \nabla \cdot (\Psi^\dagger \boldsymbol{\alpha} \Psi) \\ &= -i \frac{\gamma}{k_{\Delta}} \oint_{\partial\Omega} dS \hat{\mathbf{n}} \cdot [\nabla \Psi^\dagger (\tau_z \otimes \sigma_0) \Psi - \Psi^\dagger (\tau_z \otimes \sigma_0) \nabla \Psi] - \oint_{\partial\Omega} dS \hat{\mathbf{n}} \cdot (\Psi^\dagger \boldsymbol{\alpha} \Psi), \end{aligned} \quad (9)$$

where the Gauss's divergence theorem was implemented on the oriented surface $\partial\Omega$ with normal $\hat{\mathbf{n}}$.

Then, from the continuity equation for the conserved probability

$$\int_{\Omega} d^3x \partial_t \rho = - \int_{\Omega} d^3x \nabla \cdot \mathbf{J} = - \oint_{\partial\Omega} dS \hat{\mathbf{n}} \cdot \mathbf{J} = 0, \quad (10)$$

we identify the probability density current by the vector

$$\mathbf{J} = i \frac{\gamma}{k_{\Delta}} [\nabla \Psi^\dagger (\tau_z \otimes \sigma_0) \Psi - \Psi^\dagger (\tau_z \otimes \sigma_0) \nabla \Psi] + \Psi^\dagger \boldsymbol{\alpha} \Psi. \quad (11)$$

In this last expression, we can clearly identify two different contributions. The first one is reminiscent of the current for the non-relativistic Schrödinger equation, as can be traced back to the quadratic momentum contribution $\gamma/k_{\Delta} \mathbf{k}^2$ in the mass operator $\mathbb{M}(\mathbf{k}^2)$. On the other hand, the second contribution is proportional to the constant matrix $\boldsymbol{\alpha}$, just as in the usual relativistic Dirac formalism. It is also clear from the third identity in continuity Eq. (10) that the correct boundary condition that describes confined eigenstates within the TI-NP is given by

$$\hat{\mathbf{n}} \cdot \mathbf{J}|_{\partial\Omega} = 0. \quad (12)$$

II. SOLUTION TO THE HAMILTONIAN AT CONSTANT MASS $\mathbb{M}(\mathbf{k}) \rightarrow \Delta_0/2$

In this section, we shall consider the Dirac limit of a constant mass operator $\mathbb{M}(\mathbf{k}) \rightarrow \Delta_0/2$, such that the bulk Hamiltonian Eq. (2) reduces to

$$\hat{\mathcal{H}} \rightarrow \hat{\mathcal{H}}_{Dirac} = \frac{\Delta_0}{2} \hat{\beta} + \gamma (\boldsymbol{\alpha} \cdot \mathbf{k}). \quad (13)$$

Let us write the spinor eigenstates in the general form

$$\Psi_{nk\lambda} = \begin{pmatrix} \xi_{nk\lambda}(\mathbf{r}, \phi) \\ \chi_{nk\lambda}(\mathbf{r}, \phi) \end{pmatrix}, \quad (14)$$

where $\xi_{nk\lambda}(\mathbf{r}, \phi)$ and $\chi_{nk\lambda}(\mathbf{r}, \phi)$ are bi-spinors. Therefore, the eigenvalue problem

$$\hat{\mathcal{H}}_{Dirac} \Psi_{nk\lambda} = E \Psi_{nk\lambda} \quad (15)$$

leads to the coupled system of differential equations

$$\frac{\Delta_0}{2} \xi + \gamma (\boldsymbol{\sigma} \cdot \mathbf{k}) \chi = E \xi, \quad (16a)$$

$$\gamma (\boldsymbol{\sigma} \cdot \mathbf{k}) \xi - \frac{\Delta_0}{2} \chi = E \chi. \quad (16b)$$

Now, by decomposing the scalar product in terms of the polar coordinates eigenbasis $\hat{\mathbf{e}}_r$, $\hat{\mathbf{e}}_\phi$, and $\hat{\mathbf{e}}_z$, we have

$$\boldsymbol{\sigma} \cdot \mathbf{k} = (\boldsymbol{\sigma} \cdot \hat{\mathbf{e}}_r) (\hat{\mathbf{e}}_r \cdot \mathbf{k}) + (\boldsymbol{\sigma} \cdot \hat{\mathbf{e}}_\phi) (\hat{\mathbf{e}}_\phi \cdot \mathbf{k}) + (\boldsymbol{\sigma} \cdot \hat{\mathbf{e}}_z) (\hat{\mathbf{e}}_z \cdot \mathbf{k}), \quad (17)$$

where

$$\begin{aligned}\boldsymbol{\sigma} \cdot \hat{\mathbf{e}}_r &= \begin{pmatrix} 0 & e^{-i\phi} \\ e^{i\phi} & 0 \end{pmatrix}, \quad \boldsymbol{\sigma} \cdot \hat{\mathbf{e}}_\phi = i(\boldsymbol{\sigma} \cdot \hat{\mathbf{e}}_r) \sigma_z, \quad \boldsymbol{\sigma} \cdot \hat{\mathbf{e}}_z = \sigma_z \\ \hat{\mathbf{e}}_r \cdot \mathbf{k} &= -i\partial_r, \quad \hat{\mathbf{e}}_\phi \cdot \mathbf{k} = -\frac{i}{r}\partial_\phi \equiv \frac{1}{r}\hat{L}_z,\end{aligned}\tag{18}$$

with \hat{L}_z the z-component of the orbital angular momentum. Therefore, by conveniently re-arranging the terms in Eq. (13) we obtain

$$\hat{\mathcal{H}}_{\text{Dirac}} = \frac{\Delta_0}{2}\hat{\beta} + \gamma[\boldsymbol{\tau}_x \otimes (\boldsymbol{\sigma} \cdot \hat{\mathbf{e}}_r)] \left[-i \left(\partial_r + \frac{1}{2r} \right) + \frac{i}{r}\sigma_z \hat{J}_z \right] - i\gamma(\boldsymbol{\tau}_x \otimes \sigma_z)\partial_z,\tag{19}$$

where $\hat{J}_z = \hat{L}_z + \sigma_z/2$ is the z-component of the *total* angular momentum combining both the orbital and spin degrees of freedom. From Eq. (19), it is clear that the Hamiltonian commutes with the total angular momentum operator, which further implies that we may classify the eigenstates of $\hat{\mathcal{H}}_{\text{Dirac}}$ according the eigenvalues of the energy E , along with those of J^2 , and J_z , respectively.

Based on the previous analysis, we choose the basis Ω_λ of eigenstates of \hat{J}_z , satisfying $\hat{J}_z \Omega_\lambda = \lambda\Omega_\lambda$, as follows

$$\Omega_\lambda = \begin{pmatrix} a e^{i(\lambda-1/2)\phi} \\ b e^{i(\lambda+1/2)\phi} \end{pmatrix},\tag{20}$$

with a and b arbitrary functions of r and z , but independent of ϕ .

Now, by combining Eqs. (16), we obtain the following equation for ξ :

$$\left(E^2 - \frac{\Delta_0^2}{4} - \gamma^2 \mathbf{k}^2 \right) \xi = 0.\tag{21}$$

From the previous symmetry considerations, the bi-spinor $\xi_{nk\lambda}(\mathbf{r})$ is an eigenfunction of \hat{J}_z with the general form given by Eq. (20), as follows

$$\xi_{nk\lambda}(\mathbf{r}) = e^{ikz} \begin{pmatrix} F_{n\lambda}(r) e^{i(\lambda-1/2)\phi} \\ G_{n\lambda}(r) e^{i(\lambda+1/2)\phi} \end{pmatrix},\tag{22}$$

so that upon substitution into Eq. (21), F and G must satisfy the following differential equations

$$\frac{1}{r}\partial_r (r\partial_r F_{n\lambda}) - \frac{(\lambda-1/2)^2}{r^2} F_{n\lambda} + \left(\frac{E^2 - \Delta_0^2/4}{\gamma^2} - k^2 \right) F_{n\lambda} = 0,\tag{23a}$$

$$\frac{1}{r}\partial_r (r\partial_r G_{n\lambda}) - \frac{(\lambda+1/2)^2}{r^2} G_{n\lambda} + \left(\frac{E^2 - \Delta_0^2/4}{\gamma^2} - k^2 \right) G_{n\lambda} = 0.\tag{23b}$$

Comparing both eigenvalue equations, we conclude that (modulo an arbitrary phase)

$$G_{n\lambda}(r) = F_{n,\lambda+1}(r).\tag{24}$$

Now, let us define:

$$F_{n\lambda} = \frac{1}{\sqrt{r}} \mathcal{F}_{n\lambda}(r),\tag{25}$$

such that the eigenvalue equation reduces to

$$\frac{d^2 \mathcal{F}_{n\lambda}}{dr^2} - \frac{\lambda(\lambda-1)}{r^2} \mathcal{F}_{n\lambda} + \epsilon_{nk\lambda} \mathcal{F}_{n\lambda} = 0,\tag{26}$$

where we defined the coefficient

$$\epsilon_{nk\lambda} \equiv \frac{E_{n\lambda}^2 - \Delta_0^2/4}{\gamma^2} - k^2.\tag{27}$$

If we further define $\lambda = j + 1/2$, we obtain $\lambda(\lambda-1) = j^2 - 1/4$. Therefore,

$$\frac{d^2 \mathcal{F}_{nj}}{dr^2} - \frac{j^2 - 1/4}{r^2} \mathcal{F}_{nj} + \epsilon_{nkj} \mathcal{F}_{nj} = 0,\tag{28}$$

whose general analytical solution is given by a linear combination of Bessel functions of the first and second kind, respectively

$$\mathcal{F}_{n\lambda}(r) = \sqrt{r} (A_{nj} J_j(\sqrt{\epsilon_{nkj}} r) + B_{nj} Y_j(\sqrt{\epsilon_{nkj}} r)). \quad (29)$$

The geometry consider in the TI-NP model includes the origin $r = 0$ in the domain Ω . Therefore, we must demand regularity at $r \rightarrow 0$, and hence we conclude that $B_{nj} = 0$, since Y_j diverges in this limit. Therefore, the upper bi-spinor component ξ_{nkj} finally reduces to the analytical expression

$$\xi_{nkj}(\mathbf{r}) = A_{nj} e^{ikz} e^{ij\phi} \begin{pmatrix} J_j(\sqrt{\epsilon_{nkj}} r) \\ C_j J_{j+1}(\sqrt{\epsilon_{nkj}} r) e^{i\phi} \end{pmatrix}, \quad (30)$$

where C_j is an arbitrary constant.

The latter implies, solving for the lower bi-spinor χ_{nkj} from Eq. (16b) that

$$\chi_{nkj}(\mathbf{r}) = \frac{\gamma}{E_{nkj} + \frac{\Delta_0}{2}} (\boldsymbol{\sigma} \cdot \mathbf{k}) \xi_{nkj}(\mathbf{r}). \quad (31)$$

By applying the following identities

$$\begin{aligned} J_z \Omega_\lambda = \lambda \Omega_\lambda &\implies J_z \Omega_j = (j + 1/2) \Omega_j, \\ (\boldsymbol{\sigma} \cdot \hat{\mathbf{e}}_r) \Omega_\lambda = \begin{pmatrix} b e^{i(\lambda-1/2)\phi} \\ a e^{i(\lambda+1/2)\phi} \end{pmatrix} &\implies (\boldsymbol{\sigma} \cdot \hat{\mathbf{e}}_r) \Omega_j = \begin{pmatrix} b e^{ij\phi} \\ a e^{i(j+1)\phi} \end{pmatrix}, \end{aligned} \quad (32)$$

we get:

$$(\boldsymbol{\sigma} \cdot \mathbf{k}) \xi_{nkj}(\mathbf{r}) = e^{ikz} \begin{pmatrix} e^{ij\phi} [-iC_j (\partial_r + \frac{j+1}{r}) J_{j+1}(\sqrt{\epsilon_{nkj}} r) + kJ_j(\sqrt{\epsilon_{nkj}} r)] \\ e^{i(j+1)\phi} [-i(\partial_r - \frac{j}{r}) J_j(\sqrt{\epsilon_{nkj}} r) - kC_j J_j(\sqrt{\epsilon_{nkj}} r)] \end{pmatrix}. \quad (33)$$

By using the identities:

$$\begin{aligned} \frac{d}{dx} J_j(x) - \frac{j}{x} J_j(x) &= -J_{j+1}(x), \\ \frac{d}{dx} J_j(x) + \frac{j}{x} J_j(x) &= J_{j-1}(x), \end{aligned} \quad (34)$$

it follows that:

$$(\boldsymbol{\sigma} \cdot \mathbf{k}) \xi_{nkj}(\mathbf{r}) = e^{ikz} e^{ij\phi} \begin{pmatrix} (k - i\sqrt{\epsilon_{nkj}} C_j) J_j(\sqrt{\epsilon_{nkj}} r) \\ e^{i\phi} (i\sqrt{\epsilon_{nkj}} - kC_j) J_{j+1}(\sqrt{\epsilon_{nkj}} r) \end{pmatrix}, \quad (35)$$

and therefore:

$$\chi_{nkj}(\mathbf{r}) = \frac{\gamma}{E_{nkj} + \frac{\Delta_0}{2}} e^{ikz} e^{ij\phi} \begin{pmatrix} (k - i\sqrt{\epsilon_{nkj}} C_j) J_j(\sqrt{\epsilon_{nkj}} r) \\ e^{i\phi} (i\sqrt{\epsilon_{nkj}} - kC_j) J_{j+1}(\sqrt{\epsilon_{nkj}} r) \end{pmatrix}. \quad (36)$$

As we pointed out in Eq. 12, the mathematical condition representing quantum confinement of the electronic eigenstates within the TI-NP is that the normal current at the boundary $\partial\Omega$ vanishes, i.e. $\mathbf{n} \cdot \mathbf{J}|_{\partial\Omega} = 0$. By imposing this condition at the surfaces $z = 0$ and $z = h$, i.e. $\hat{\mathbf{e}}_z \cdot \mathbf{J}|_{z=\{0,h\}} = 0$, we are led to construct linear combinations from the basic solutions of the form $e^{ikz} - e^{-ikz} \propto \sin(kz)$, to obtain a quantization of the z -component of the momentum k

$$k = \frac{m\pi}{h}, \quad m = 1, 2, \dots \quad (37)$$

The analogous condition at the lateral surfaces of the wedge $\phi = 0$ and $\phi = \alpha$, i.e. $\hat{\mathbf{e}}_\phi \cdot \mathbf{J}|_{\phi=\{0,\alpha\}} = 0$, leads to linear combinations of the basic solutions of the form $e^{ij\phi} - e^{-ij\phi} \propto \sin(j\phi)$, with the corresponding quantization of the index j

$$j = \frac{l\pi}{\alpha}, \quad l = 1, 2, \dots \quad (38)$$

Finally, imposing the confinement condition at the external radial surface $r = R$, i.e. $\hat{\mathbf{e}}_r \cdot \mathbf{J}|_{r=R} = 0$ leads to the equation

$$J_{\frac{l\pi}{\alpha}}(\kappa R) J_{\frac{l\pi}{\alpha}+1}(\kappa R) = 0, \quad (39)$$

where the quantization condition Eq. (38) over j was explicitly implemented in terms of the integer l .

Therefore, the full energy spectrum in the constant mass limit is

$$E_{nml}^\pm = \pm \sqrt{\frac{\Delta_0^2}{4} + \gamma^2 \left(\frac{m^2 \pi^2}{h^2} + \frac{\kappa_{nl}^2}{R^2} \right)}, \quad (40)$$

where $\kappa_{nl} = \kappa R$ are the (infinitely-many) solutions of Eq. (39).

III. ANALYTICAL SOLUTION TO THE HAMILTONIAN WITH FULL MASS OPERATOR $\mathbb{M}(\mathbf{k})$

In this case, the full Hamiltonian reads:

$$\hat{\mathcal{H}} = \mathbb{M}(\mathbf{k})\hat{\beta} + \gamma(\boldsymbol{\alpha} \cdot \mathbf{k}), \quad (41)$$

with $\mathbb{M}(\mathbf{k})$ the full mass operator defined in Eq. (1). As in Sec. 2, we look for the spinor solutions $\Psi_{nk\lambda} = (\varphi, \chi)^T$ to the eigenvalue problem

$$\hat{\mathcal{H}}\Psi_{nk\lambda} = E\Psi_{nk\lambda}, \quad (42)$$

that leads to the coupled system of differential equations

$$[\mathbb{M}(\mathbf{k}) - E]\varphi + \gamma(\boldsymbol{\sigma} \cdot \mathbf{k})\chi = 0, \quad (43a)$$

$$\gamma(\boldsymbol{\sigma} \cdot \mathbf{k})\varphi - [\mathbb{M}(\mathbf{k}) + E]\chi = 0. \quad (43b)$$

To solve the problem, based on the explicit analytical solution obtained for the constant mass case presented in Sec.2, we follow the ansatz:

$$\varphi = e^{ikz} \begin{pmatrix} c_1 e^{ij\phi} J_j(\kappa r) \\ c_2 e^{i(j+1)\phi} J_{j+1}(\kappa r) \end{pmatrix}, \quad (44a)$$

$$\chi = e^{ikz} \begin{pmatrix} c_3 e^{ij\phi} J_j(\kappa r) \\ c_4 e^{i(j+1)\phi} J_{j+1}(\kappa r) \end{pmatrix}, \quad (44b)$$

where $J_j(\kappa r)$ are Bessel functions of the first kind and of order j , and the coefficient κ is to be determined later from the confinement boundary conditions defined by Eq. (12). By inserting Eq. (44) into Eq. (43a), we obtain

$$\gamma(\boldsymbol{\sigma} \cdot \mathbf{k})\chi = e^{ikz}\gamma \left[(\hat{\mathbf{e}}_r \cdot \boldsymbol{\sigma}) \begin{pmatrix} -ic_3 e^{ij\phi} \left(\partial_r - \frac{j}{r} \right) J_j(\kappa r) \\ -ic_4 e^{i(j+1)\phi} \left(\partial_r + \frac{j+1}{r} \right) J_{j+1}(\kappa r) \end{pmatrix} + k \begin{pmatrix} c_3 e^{ij\phi} J_j(\kappa r) \\ -c_4 e^{i(j+1)\phi} J_{j+1}(\kappa r) \end{pmatrix} \right]. \quad (45)$$

Applying the basic Bessel function identities

$$\left(\partial_r - \frac{j}{r} \right) J_j(\kappa r) = -\kappa J_{j+1}(\kappa r), \quad (46a)$$

$$\left(\partial_r + \frac{j+1}{r} \right) J_{j+1}(\kappa r) = \kappa J_j(\kappa r), \quad (46b)$$

it follows that:

$$\gamma(\boldsymbol{\sigma} \cdot \mathbf{k})\chi = e^{ikz}\gamma \begin{pmatrix} (kc_3 - i\kappa c_4) e^{ij\phi} J_j(\kappa r) \\ (i\kappa c_3 - kc_4) e^{i(j+1)\phi} J_{j+1}(\kappa r) \end{pmatrix}. \quad (47)$$

Following a similar algebra, we also obtain

$$\gamma(\boldsymbol{\sigma} \cdot \mathbf{k})\varphi = e^{ikz}\gamma \begin{pmatrix} (kc_1 - i\kappa c_2) e^{ij\phi} J_j(\kappa r) \\ (i\kappa c_1 - kc_2) e^{i(j+1)\phi} J_{j+1}(\kappa r) \end{pmatrix}. \quad (48)$$

Additionally, it is straightforward to obtain the result

$$\begin{aligned} [\mathbb{M}(\mathbf{k}) - E]\varphi &= e^{ikz} \left[\frac{\Delta_0}{2} + \frac{\gamma}{k_\Delta} k^2 - E - \frac{\gamma}{k_\Delta} \left(\partial_r^2 + \frac{1}{r} \partial_r - \frac{\hat{L}_z^2}{r^2} \right) \right] \begin{pmatrix} c_1 e^{ij\phi} J_j(\kappa r) \\ c_2 e^{i(j+1)\phi} J_{j+1}(\kappa r) \end{pmatrix} \\ &= \left(\frac{\Delta_0}{2} + \frac{\gamma}{k_\Delta} k^2 - E - \frac{\gamma}{k_\Delta} \kappa^2 \right) \varphi, \end{aligned} \quad (49)$$

where the following Bessel function identities were applied

$$\left(\partial_r^2 + \frac{1}{r}\partial_r - \frac{j^2}{r}\right) J_j(\kappa r) = -\kappa^2 J_j(\kappa r), \quad (50a)$$

$$\left(\partial_r^2 + \frac{1}{r}\partial_r - \frac{(j+1)^2}{r}\right) J_{j+1}(\kappa r) = -\kappa^2 J_{j+1}(\kappa r). \quad (50b)$$

From similar algebraic procedure, we also obtain the result

$$[\mathbb{M}(\mathbf{k}) + E]\chi = \left(\frac{\Delta_0}{2} + \frac{\gamma}{k_\Delta}k^2 + E + \frac{\gamma}{k_\Delta}\kappa^2\right)\chi. \quad (51)$$

A. Eigenvalues

Combining the partial results in the previous subsection, the eigenvalue system of Eq. (43a) and Eq. (43b) reduces to the linear algebraic system

$$\mathbb{A}(\kappa, E)\mathbf{c} = 0, \quad (52)$$

where we arranged the coefficients in the vector $\mathbf{c} = (c_1, c_2, c_3, c_4)^T$, and we also defined the matrix

$$\mathbb{A}(\kappa, E) = \begin{bmatrix} \Lambda - E & 0 & k\gamma & -i\kappa\gamma \\ 0 & \Lambda - E & i\kappa\gamma & -k\gamma \\ k\gamma & -i\kappa\gamma & -(\Lambda + E) & 0 \\ i\kappa\gamma & -k\gamma & 0 & -(\Lambda + E) \end{bmatrix}, \quad (53)$$

with

$$\Lambda = \frac{\Delta_0}{2} + \frac{\gamma}{k_\Delta}(k^2 + \kappa^2). \quad (54)$$

The linear system possesses nontrivial solutions if $\det \mathbb{A} = 0$, which implies the secular fourth-degree polynomial equation for the eigenvalues

$$[\Lambda^2 - E^2 + \gamma^2(k^2 + \kappa^2)]^2 = 0. \quad (55)$$

Solving for the energy eigenvalues, we obtain

$$E_{\pm} = \pm \sqrt{\left(\frac{\Delta_0}{2} + \frac{\gamma}{k_\Delta}(k^2 + \kappa^2)\right)^2 + \gamma^2(k^2 + \kappa^2)}. \quad (56)$$

1. Current density and confining boundary condition

As derived in detail in Sec. 1, the mathematical expression for the probability density current is

$$\mathbf{J} = i\frac{\gamma}{k_\Delta} [\nabla\Psi^\dagger (\tau_z \otimes \sigma_0) \Psi - \Psi^\dagger (\tau_z \otimes \sigma_0) \nabla\Psi] + \Psi^\dagger \boldsymbol{\alpha} \Psi. \quad (57)$$

The more general boundary condition that leads to confinement, as discussed in Sec. 1 (and in the main text) involves the vanishing of the normal component of the current at the surface $\partial\Omega$ of the nanoparticle, i.e. $\hat{\mathbf{n}} \cdot \mathbf{J}|_{\partial\Omega} = 0$. By imposing this condition at the surfaces $z = 0$ and $z = h$, i.e. $\hat{\mathbf{e}}_z \cdot \mathbf{J}|_{z=\{0,h\}} = 0$, we are led to construct linear combinations from the basic solutions of the form $e^{ikz} - e^{-ikz} \propto \sin(kz)$, to obtain a quantization of the z -component of the momentum k

$$k = \frac{m\pi}{h}, \quad m = 1, 2, \dots \quad (58)$$

The analogous condition at the lateral surfaces of the wedge $\phi = 0$ and $\phi = \alpha$, i.e. $\hat{\mathbf{e}}_\phi \cdot \mathbf{J}|_{\phi=\{0,\alpha\}} = 0$, leads to linear combinations of the basic solutions of the form $e^{ij\phi} - e^{-ij\phi} \propto \sin(j\phi)$, with the corresponding quantization of the index j

$$j = \frac{l\pi}{\alpha}, \quad l = 1, 2, \dots \quad (59)$$

Finally for the surface $r = R$ we have

$$\hat{\mathbf{e}}_r \cdot \mathbf{J}|_{r=R} = 0. \quad (60)$$

Applying this condition to Eq. (57), we obtain a linear combination of two terms. The first one is

$$i \frac{\gamma}{k_\Delta} [(\partial_r \Psi^\dagger) (\tau_z \otimes \sigma_0) \Psi - \Psi^\dagger (\tau_z \otimes \sigma_0) \partial_r \Psi]. \quad (61)$$

The second term involves the matrix form

$$\begin{aligned} \hat{\mathbf{e}}_r \cdot \boldsymbol{\alpha} &= \alpha_x (\hat{\mathbf{e}}_x \cdot \hat{\mathbf{e}}_r) + \alpha_y (\hat{\mathbf{e}}_y \cdot \hat{\mathbf{e}}_r) \\ &= \cos \phi \alpha_x + \sin \phi \alpha_y \\ &= \gamma \cos \phi (\tau_x \otimes \sigma_x) + 2\gamma \sin \phi (\tau_x \otimes \sigma_y) \\ &= \gamma \tau_x \otimes \begin{pmatrix} 0 & e^{-i\phi} \\ e^{i\phi} & 0 \end{pmatrix}. \end{aligned} \quad (62)$$

Then, combining both expressions, the boundary condition at the radial surface $r = R$ in Eq. (60) reduces to

$$i \frac{\gamma}{k_\Delta} [(\partial_r \Psi^\dagger) (\tau_z \otimes \sigma_0) \Psi - \Psi^\dagger (\tau_z \otimes \sigma_0) \partial_r \Psi] + \gamma \Psi^\dagger \tau_x \otimes \begin{pmatrix} 0 & e^{-i\phi} \\ e^{i\phi} & 0 \end{pmatrix} \Psi \Big|_{r=R} = 0. \quad (63)$$

From the form of Eqs. (44), we directly obtain

$$(\partial_r \Psi^\dagger) (\tau_z \otimes \sigma_0) \Psi - \Psi^\dagger (\tau_z \otimes \sigma_0) \partial_r \Psi = 0, \quad (64)$$

and then Eq. (63) reduces to

$$(c_1 c_4^* + c_2^* c_3 + c_1^* c_4 + c_2 c_3^*) J_{\frac{l_x}{\alpha}}(\kappa R) J_{\frac{l_x}{\alpha}+1}(\kappa R) = 0, \quad (65)$$

where the quantization over j was implemented in terms of l . This clearly leads to the same Eq. (39) previously obtained in Sec. 2 for the constant mass limit.

Therefore, if $\kappa_{nl} = R\kappa$ are the solutions of Eq. (39), the eigenvalues of the problem are:

$$E_{nml}^\pm = \pm \sqrt{\left[\frac{\Delta_0}{2} + \frac{\gamma}{k_\Delta} \left(\frac{m^2 \pi^2}{h^2} + \frac{\kappa_{nl}^2}{R^2} \right) \right]^2 + \gamma^2 \left(\frac{m^2 \pi^2}{h^2} + \frac{\kappa_{nl}^2}{R^2} \right)}. \quad (66)$$

B. Eigenvectors

The four eigenvectors associated to Eq. (52) are:

$$\begin{pmatrix} i \frac{\kappa (-M \pm \sqrt{M^2 + \gamma^2 (k^2 + \kappa^2)})}{\gamma (k^2 + \kappa^2)} \\ \frac{k (-M \pm \sqrt{M^2 + \gamma^2 (k^2 + \kappa^2)})}{\gamma (k^2 + \kappa^2)} \\ 0 \\ 1 \end{pmatrix}, \quad \begin{pmatrix} \frac{k (M \pm \sqrt{M^2 + \gamma^2 (k^2 + \kappa^2)})}{\gamma (k^2 + \kappa^2)} \\ i \frac{\kappa (M \pm \sqrt{M^2 + \gamma^2 (k^2 + \kappa^2)})}{\gamma (k^2 + \kappa^2)} \\ 1 \\ 0 \end{pmatrix}. \quad (67)$$

These four solutions are degenerated by pairs. Then, by defining the coefficients

$$\begin{aligned} \mathcal{M} &= \frac{M}{\gamma (k^2 + \kappa^2)}, \\ \widetilde{\mathcal{M}} &= \frac{\sqrt{M^2 + \gamma^2 (k^2 + \kappa^2)}}{\gamma (k^2 + \kappa^2)}, \end{aligned} \quad (68)$$

we obtain the four independent spinor eigenstates

$$|nml; 1^\pm\rangle = \begin{pmatrix} i\kappa(-\mathcal{M} \pm \widetilde{\mathcal{M}})J_{\frac{l\pi}{\alpha}}(\kappa r) \\ k(-\mathcal{M} \pm \widetilde{\mathcal{M}})J_{\frac{l\pi}{\alpha}+1}(\kappa r)e^{i\phi} \\ 0 \\ J_{\frac{l\pi}{\alpha}+1}(\kappa r)e^{i\phi} \end{pmatrix}, \quad (69)$$

$$|nml; 2^\pm\rangle = \begin{pmatrix} k(\mathcal{M} \pm \widetilde{\mathcal{M}})J_{\frac{l\pi}{\alpha}}(\kappa r) \\ i\kappa(\mathcal{M} \pm \widetilde{\mathcal{M}})J_{\frac{l\pi}{\alpha}+1}(\kappa r)e^{i\phi} \\ J_{\frac{l\pi}{\alpha}}(\kappa r) \\ 0 \end{pmatrix}. \quad (70)$$

Therefore, the general solution can be written as a linear combination of the four orthogonal solutions

$$\Psi_{nml}(\mathbf{r}) = \sin\left(\frac{m\pi}{h}z\right) \sin\left(\frac{l\pi}{\alpha}\phi\right) \sum_{s=\pm} \left[A_s \begin{pmatrix} i\kappa(-\mathcal{M} + s\widetilde{\mathcal{M}})J_{\frac{l\pi}{\alpha}}(\kappa r) \\ k(-\mathcal{M} + s\widetilde{\mathcal{M}})J_{\frac{l\pi}{\alpha}+1}(\kappa r)e^{i\phi} \\ 0 \\ J_{\frac{l\pi}{\alpha}+1}(\kappa r)e^{i\phi} \end{pmatrix} + B_s \begin{pmatrix} k(\mathcal{M} + s\widetilde{\mathcal{M}})J_{\frac{l\pi}{\alpha}}(\kappa r) \\ i\kappa(\mathcal{M} + s\widetilde{\mathcal{M}})J_{\frac{l\pi}{\alpha}+1}(\kappa r)e^{i\phi} \\ J_{\frac{l\pi}{\alpha}}(\kappa r) \\ 0 \end{pmatrix} \right] \quad (71)$$

C. Normalization

Let us now calculate the normalization coefficients for each of the four orthogonal spinor eigenstates. For notational simplicity, let us define the parameters

$$\nu = \frac{l\pi}{\alpha}, \quad u = \frac{m\pi}{h}, \quad \kappa = \frac{\kappa_{nml}}{R}. \quad (72)$$

The normalization condition for the coefficients A_s in Eq. (71) is

$$\begin{aligned} 1 &= |A_\pm|^2 \int d^3\mathbf{r} \sin^2(uz) \sin^2(\nu\phi) \left[\left| \kappa(-\mathcal{M} \pm \widetilde{\mathcal{M}}) \right|^2 J_\nu^2(\kappa r) + \left(\left| k(-\mathcal{M} \pm \widetilde{\mathcal{M}}) \right|^2 + 1 \right) J_{\nu+1}^2(\kappa r) \right] \\ &= |A_\pm|^2 \frac{\alpha h}{4} \left[\left| \kappa(-\mathcal{M} \pm \widetilde{\mathcal{M}}) \right|^2 \int_0^R dr r J_\nu^2(\kappa r) + \left(\left| k(-\mathcal{M} \pm \widetilde{\mathcal{M}}) \right|^2 + 1 \right) \int_0^R dr r J_{\nu+1}^2(\kappa r) \right] \\ &= |A_\pm|^2 \frac{\alpha h}{4} \left[\left| \kappa(-\mathcal{M} \pm \widetilde{\mathcal{M}}) \right|^2 (J_\nu^2(\kappa R) - J_{\nu+1}(\kappa R)J_{\nu-1}(\kappa R)) \right. \\ &\quad \left. + \left(\left| k(-\mathcal{M} \pm \widetilde{\mathcal{M}}) \right|^2 + 1 \right) (J_{\nu+1}^2(\kappa R) - J_{\nu+2}(\kappa R)J_\nu(\kappa R)) \right], \end{aligned} \quad (73)$$

and therefore, choosing the arbitrary phase for them to be real, we obtain

$$\begin{aligned} A_\pm &= \sqrt{\frac{4}{\alpha h}} \left[\left| \kappa(-\mathcal{M} \pm \widetilde{\mathcal{M}}) \right|^2 (J_\nu^2(\kappa R) - J_{\nu+1}(\kappa R)J_{\nu-1}(\kappa R)) \right. \\ &\quad \left. + \left(\left| k(-\mathcal{M} \pm \widetilde{\mathcal{M}}) \right|^2 + 1 \right) (J_{\nu+1}^2(\kappa R) - J_{\nu+2}(\kappa R)J_\nu(\kappa R)) \right]^{-1/2}. \end{aligned} \quad (74)$$

Similarly, for the B_s normalization coefficients in Eq. (71) we obtain

$$B_{\pm} = \sqrt{\frac{4}{\alpha h}} \left[\left(|k(\mathcal{M} \pm \widetilde{\mathcal{M}})|^2 + 1 \right) (J_{\nu}^2(\kappa R) - J_{\nu+1}(\kappa R)J_{\nu-1}(\kappa R)) \right. \\ \left. + |\kappa(\mathcal{M} \pm \widetilde{\mathcal{M}})|^2 (J_{\nu+1}^2(\kappa R) - J_{\nu+2}(\kappa R)J_{\nu}(\kappa R)) \right]^{-1/2}. \quad (75)$$

IV. SELECTION RULES

In this section, we analyze the optical transitions, along with the corresponding selection rules, within the standard dipolar approximation for the electric field. For this purpose, we consider the matrix elements of the total electric dipole operator[1, 2]

$$\mathbf{d} = e\mathbf{r}(\tau_0 \otimes \sigma_0) + \frac{eR_0}{2}(\tau_y \otimes \boldsymbol{\sigma}), \quad (76)$$

where the first term represents the intra-band contribution, arising from the envelope wavefunctions multiplying the same basis state in the $\mathbf{k} \cdot \mathbf{p}$ approximation for the bulk band structure[1–3]. On the other hand, the second term in Eq. (76) accounts for transitions between different $\mathbf{k} \cdot \mathbf{p}$ basis states[1–3].

Let us define the probability amplitude for an optical transition along the $\hat{\mathbf{e}}_{\mu}$ -direction, by the matrix element

$$T_{\mu}(|i\rangle \rightarrow |f\rangle) = \langle n'm'l'; f | \hat{\mathbf{e}}_{\mu} \cdot \mathbf{d} | nml; i \rangle, \quad (77)$$

where i, f denotes each of the four possible eigenstates labelled by the indexes $q = 1, 2$ and $s = \pm$, as defined in the previous section. We shall discuss our analytical results for the transition amplitudes in different orthogonal directions.

A. Master integrals

Let us define the following integrals

$$\int_0^{\alpha} d\phi \sin\left(\frac{l\pi}{\alpha}\phi\right) \sin\left(\frac{l'\pi}{\alpha}\phi\right) = \frac{\alpha}{2}\delta_{ll'}. \quad (78)$$

$$\int_0^h dz \sin\left(\frac{m\pi}{h}z\right) \sin\left(\frac{m'\pi}{h}z\right) = \frac{h}{2}\delta_{mm'}. \quad (79)$$

$$I_z \equiv \int_0^h dz z \sin\left(\frac{m\pi}{h}z\right) \sin\left(\frac{m'\pi}{h}z\right) \\ = \frac{h^2}{2\pi^2} \left[\frac{\cos(\pi\Delta m) - 1}{\Delta m^2} - \frac{\cos(\pi M) - 1}{M^2} + \frac{\pi \sin(\pi\Delta m) - 1}{\Delta m} + \frac{\pi \sin(\pi M) - 1}{M} \right] \\ = \begin{cases} 0 & \text{if } \Delta m \neq 0 \text{ and } M \neq 0 \in \mathbb{Z} \text{ are even integers.} \\ 4h^2/\pi^2 (1/\Delta m^2 - 1/M^2) & \text{If } \Delta m \text{ and } M \text{ are odd integers} \\ h^2/4 & \text{if } \Delta m = 0 \text{ and } M \neq 0 \text{ (even)} \\ -h^2/4 & \text{if } M = 0 \text{ and } \Delta m \neq 0 \text{ (even)} \end{cases}, \quad (80)$$

where $\Delta m = m' - m$ and $M = m' + m$. Also, in order to have a non-vanishing integral, Δm and M must have the same parity.

$$I_n' \equiv \int_0^R dr r J_j(\kappa' r) J_j(\kappa r) \\ = R^2 \int_0^1 dx x J_j(\kappa' R x) J_j(\kappa R x) \\ = R \frac{\kappa J_{j-1}(\kappa R) J_j(\kappa' R) - \kappa' J_{j-1}(\kappa' R) J_j(\kappa R)}{\kappa^2 - \kappa'^2}. \quad (81)$$

$$\begin{aligned}
\tilde{\mathbf{I}}_n^{n'} &\equiv \int_0^R dr r J_{j+1}(\kappa' r) J_{j+1}(\kappa r) \\
&= R^2 \int_0^1 dx x J_{j+1}(\kappa' R x) J_{j+1}(\kappa R x) \\
&= R \frac{\kappa J_j(\kappa R) J_{j+1}(\kappa' R) - \kappa' J_j(\kappa' R) J_{j+1}(\kappa R)}{\kappa^2 - \kappa'^2}.
\end{aligned} \tag{82}$$

where the well-known properties of the Bessel functions were used [4].

$$\mathbf{J}_{nl}^{n'l'} \equiv \int_0^R dr r^2 J_j(\kappa r) J_{j'}(\kappa' r). \tag{83}$$

$$\tilde{\mathbf{J}}_{nl}^{n'l'} \equiv \int_0^R dr r^2 J_{j+1}(\kappa r) J_{j'+1}(\kappa' r). \tag{84}$$

$$\mathbf{K}_{nl}^{n'l'} \equiv \int_0^R dr r J_j(\kappa r) J_{j'+1}(\kappa' r) \tag{85}$$

$$\tilde{\mathbf{K}}_{nl}^{n'l'} \equiv \int_0^R dr r J_{j+1}(\kappa r) J_{j'}(\kappa' r) \tag{86}$$

The integrals $\mathbf{J}_{nl}^{n'l'}$, $\tilde{\mathbf{J}}_{nl}^{n'l'}$, $\mathbf{K}_{nl}^{n'l'}$, and $\tilde{\mathbf{K}}_{nl}^{n'l'}$ cannot be expressed in a closed analytical form, and hence are evaluated numerically.

$$\begin{aligned}
\mathbf{I}_\phi^\pm &\equiv \int_0^\alpha d\phi e^{\pm i\phi} \sin\left(\frac{l\pi}{\alpha}\phi\right) \sin\left(\frac{l'\pi}{\alpha}\phi\right) \\
&= \frac{\alpha}{2(\pi^2 \Delta l^2 - \alpha^2)} \left\{ e^{\pm i\alpha} [\pi \Delta l \sin(\pi \Delta l) \pm i\alpha \cos(\pi \Delta l)] \mp i\alpha \right\} \\
&\quad - \frac{\alpha}{2(\pi^2 L^2 - \alpha^2)} \left\{ e^{\pm i\alpha} [\pi L \sin(\pi L) \pm i\alpha \cos(\pi L)] \mp i\alpha \right\}
\end{aligned} \tag{87}$$

where $\Delta l = l' - l$ and $L = l + l'$.

B. Selection rules in z -direction

$$\begin{aligned}
& T_z(|1^\pm\rangle \rightarrow |1^\pm\rangle) \\
&= eA_\pm A'_\pm \int d^3\mathbf{r} \sin(kz) \sin(k'z) \sin(j\phi) \sin(j'\phi) \\
&\times \left\{ \kappa\kappa' \left(-\mathcal{M} \pm \widetilde{\mathcal{M}} \right) \left(-\mathcal{M}' \pm \widetilde{\mathcal{M}}' \right) z J_j(\kappa r) J_{j'}(\kappa' r) \right. \\
&+ \left[\kappa\kappa' \left(-\mathcal{M} \pm \widetilde{\mathcal{M}} \right) \left(-\mathcal{M}' \pm \widetilde{\mathcal{M}}' \right) + 1 \right] z J_{j+1}(\kappa r) J_{j'+1}(\kappa' r) \\
&+ \left. \frac{iR_0}{2} \left[k' \left(-\mathcal{M}' \pm \widetilde{\mathcal{M}}' \right) - k \left(-\mathcal{M} \pm \widetilde{\mathcal{M}} \right) \right] J_{j+1}(\kappa r) J_{j'+1}(\kappa' r) \right\} \\
&= \frac{e\alpha}{2} A_\pm A'_\pm \delta_{ll'} \left\{ \kappa\kappa' \left(-\mathcal{M} \pm \widetilde{\mathcal{M}} \right) \left(-\mathcal{M}' \pm \widetilde{\mathcal{M}}' \right) \Gamma_n^{l'} \mathbf{I}_z(\Delta m, M) \right. \\
&+ \left[\kappa\kappa' \left(-\mathcal{M} \pm \widetilde{\mathcal{M}} \right) \left(-\mathcal{M}' \pm \widetilde{\mathcal{M}}' \right) + 1 \right] \widetilde{\Gamma}_n^{l'} \mathbf{I}_z(\Delta m, M) \\
&+ \left. \frac{i\hbar R_0}{4} \delta_{mm'} \left[k' \left(-\mathcal{M}' \pm \widetilde{\mathcal{M}}' \right) - k \left(-\mathcal{M} \pm \widetilde{\mathcal{M}} \right) \right] \widetilde{\Gamma}_n^{l'} \right\}. \tag{88}
\end{aligned}$$

The following matrix gives the values of the first 64 elements of the transition $|T_z|$ between $|111; 1^+\rangle \rightarrow |nm1, 1^+\rangle$ for a nano-particle made of Bi_2Te_3 with $R = 10\text{nm}$, $h = 1\text{nm}$, $\alpha = \pi/6$:

$$\begin{pmatrix}
8 & 2.88091 & 0 & 0.23035 & 0 & 0.0634495 & 0 & 0.0261078 \\
7.33474 & 2.64153 & 0 & 0.211215 & 0 & 0.0581791 & 0 & 0.0239392 \\
0 & 0 & 0 & 0 & 0 & 0 & 0 & 0 \\
1.96007 & 0.706002 & 0 & 0.0564561 & 0 & 0.015551 & 0 & 0.00639883 \\
0 & 0 & 0 & 0 & 0 & 0 & 0 & 0 \\
1.24078 & 0.446931 & 0 & 0.0357421 & 0 & 0.00984537 & 0 & 0.00405114 \\
0 & 0 & 0 & 0 & 0 & 0 & 0 & 0 \\
0.936291 & 0.337241 & 0 & 0.026972 & 0 & 0.00742969 & 0 & 0.00305715
\end{pmatrix} \tag{89}$$

$$\begin{aligned}
& T_z(|2^\pm\rangle \rightarrow |2^\pm\rangle) \\
&= eB_\pm B'_\pm \int d^3\mathbf{r} \sin(kz) \sin(k'z) \sin(j\phi) \sin(j'\phi) \\
&\times \left\{ \kappa\kappa' \left(\mathcal{M} \pm \widetilde{\mathcal{M}} \right) \left(\mathcal{M}' \pm \widetilde{\mathcal{M}}' \right) z J_{j+1}(\kappa r) J_{j'+1}(\kappa' r) \right. \\
&+ \left[\kappa\kappa' \left(\mathcal{M} \pm \widetilde{\mathcal{M}} \right) \left(\mathcal{M}' \pm \widetilde{\mathcal{M}}' \right) + 1 \right] z J_j(\kappa r) J_{j'}(\kappa' r) \\
&+ \left. \frac{iR_0}{2} \left[k \left(\mathcal{M} \pm \widetilde{\mathcal{M}} \right) - k' \left(\mathcal{M}' \pm \widetilde{\mathcal{M}}' \right) \right] J_j(\kappa r) J_{j'}(\kappa' r) \right\} \\
&= \frac{e\alpha}{2} B_\pm B'_\pm \delta_{ll'} \left\{ \kappa\kappa' \left(\mathcal{M} \pm \widetilde{\mathcal{M}} \right) \left(\mathcal{M}' \pm \widetilde{\mathcal{M}}' \right) \widetilde{\Gamma}_n^{l'} \mathbf{I}_z(\Delta m, M) \right. \\
&+ \left[\kappa\kappa' \left(\mathcal{M} \pm \widetilde{\mathcal{M}} \right) \left(\mathcal{M}' \pm \widetilde{\mathcal{M}}' \right) + 1 \right] \Gamma_n^{l'} \mathbf{I}_z(\Delta m, M) \\
&+ \left. \frac{i\hbar R_0}{4} \delta_{mm'} \left[k \left(\mathcal{M} \pm \widetilde{\mathcal{M}} \right) - k' \left(\mathcal{M}' \pm \widetilde{\mathcal{M}}' \right) \right] \Gamma_n^{l'} \right\}. \tag{90}
\end{aligned}$$

$$\begin{aligned}
& T_z(|1^\pm\rangle \rightarrow |1^\mp\rangle) \\
&= eA_\pm A'_\mp \int d^3\mathbf{r} \sin(kz) \sin(k'z) \sin(j\phi) \sin(j'\phi) \\
&\times \left\{ \kappa\kappa' \left(-\mathcal{M} \pm \widetilde{\mathcal{M}} \right) \left(-\mathcal{M}' \mp \widetilde{\mathcal{M}}' \right) z J_j(\kappa r) J_{j'}(\kappa' r) \right. \\
&+ \left[\kappa\kappa' \left(-\mathcal{M} \pm \widetilde{\mathcal{M}} \right) \left(-\mathcal{M}' \mp \widetilde{\mathcal{M}}' \right) + 1 \right] z J_{j+1}(\kappa r) J_{j'+1}(\kappa' r) \\
&+ \left. \frac{iR_0}{2} \left[k' \left(-\mathcal{M}' \mp \widetilde{\mathcal{M}}' \right) - k \left(-\mathcal{M} \pm \widetilde{\mathcal{M}} \right) \right] J_{j+1}(\kappa r) J_{j'+1}(\kappa' r) \right\} \\
&= \frac{e\alpha}{2} A_\pm A'_\mp \delta_{ll'} \left\{ \kappa\kappa' \left(-\mathcal{M} \pm \widetilde{\mathcal{M}} \right) \left(-\mathcal{M}' \mp \widetilde{\mathcal{M}}' \right) \Gamma_n^{n'} \mathbb{I}_z(\Delta m, M) \right. \\
&+ \left[\kappa\kappa' \left(-\mathcal{M} \pm \widetilde{\mathcal{M}} \right) \left(-\mathcal{M}' \mp \widetilde{\mathcal{M}}' \right) + 1 \right] \widetilde{\Gamma}_n^{n'} \mathbb{I}_z(\Delta m, M) \\
&+ \left. \frac{i\hbar R_0}{4} \delta_{mm'} \left[k' \left(-\mathcal{M}' \mp \widetilde{\mathcal{M}}' \right) - k \left(-\mathcal{M} \pm \widetilde{\mathcal{M}} \right) \right] \widetilde{\Gamma}_n^{n'} \right\}. \tag{91}
\end{aligned}$$

$$\begin{aligned}
& T_z(|2^\pm\rangle \rightarrow |2^\mp\rangle) \\
&= eB_\pm B'_\mp \int d^3\mathbf{r} \sin(kz) \sin(k'z) \sin(j\phi) \sin(j'\phi) \\
&\times \left\{ \kappa\kappa' \left(\mathcal{M} \pm \widetilde{\mathcal{M}} \right) \left(\mathcal{M}' \mp \widetilde{\mathcal{M}}' \right) z J_{j+1}(\kappa r) J_{j'+1}(\kappa' r) \right. \\
&+ \left[\kappa\kappa' \left(\mathcal{M} \pm \widetilde{\mathcal{M}} \right) \left(\mathcal{M}' \mp \widetilde{\mathcal{M}}' \right) + 1 \right] z J_j(\kappa r) J_{j'}(\kappa' r) \\
&+ \left. \frac{iR_0}{2} \left[k \left(\mathcal{M} \pm \widetilde{\mathcal{M}} \right) - k' \left(\mathcal{M}' \mp \widetilde{\mathcal{M}}' \right) \right] J_j(\kappa r) J_{j'}(\kappa' r) \right\} \\
&= \frac{e\alpha}{2} B_\pm B'_\mp \delta_{ll'} \left\{ \kappa\kappa' \left(\mathcal{M} \pm \widetilde{\mathcal{M}} \right) \left(\mathcal{M}' \mp \widetilde{\mathcal{M}}' \right) \widetilde{\Gamma}_n^{n'} \mathbb{I}_z(\Delta m, M) \right. \\
&+ \left[\kappa\kappa' \left(\mathcal{M} \pm \widetilde{\mathcal{M}} \right) \left(\mathcal{M}' \mp \widetilde{\mathcal{M}}' \right) + 1 \right] \Gamma_n^{n'} \mathbb{I}_z(\Delta m, M) \\
&+ \left. \frac{i\hbar R_0}{4} \delta_{mm'} \left[k \left(\mathcal{M} \pm \widetilde{\mathcal{M}} \right) - k' \left(\mathcal{M}' \mp \widetilde{\mathcal{M}}' \right) \right] \Gamma_n^{n'} \right\}. \tag{92}
\end{aligned}$$

$$\begin{aligned}
& T_z(|1^\pm\rangle \rightarrow |2^\pm\rangle) \\
&= eA_\pm B'_\pm \int d^3\mathbf{r} \sin(kz) \sin(k'z) \sin(j\phi) \sin(j'\phi) \\
&\times \left\{ i \left(\mathcal{M}' \pm \widetilde{\mathcal{M}}' \right) \left(-\mathcal{M} \pm \widetilde{\mathcal{M}} \right) z \left[k' \kappa J_j(\kappa r) J_{j'}(\kappa' r) - \kappa \kappa' J_{j+1}(\kappa r) J_{j'+1}(\kappa' r) \right] \right. \\
&+ \left. \frac{R_0}{2} \left[\kappa' \left(\mathcal{M}' \pm \widetilde{\mathcal{M}}' \right) J_{j+1}(\kappa r) J_{j'+1}(\kappa' r) - \kappa \left(-\mathcal{M} \pm \widetilde{\mathcal{M}} \right) J_j(\kappa r) J_{j'}(\kappa' r) \right] \right\} \\
&= \frac{e\alpha}{2} A_\pm B'_\pm \delta_{ll'} \left\{ i \left(\mathcal{M}' \pm \widetilde{\mathcal{M}}' \right) \left(-\mathcal{M} \pm \widetilde{\mathcal{M}} \right) \left[k' \kappa \Gamma_n^{n'} - \kappa \kappa' \widetilde{\Gamma}_n^{n'} \right] \mathbb{I}_z(\Delta m, M) \right. \\
&+ \left. \frac{\hbar R_0}{4} \delta_{mm'} \left[\kappa' \left(\mathcal{M}' \pm \widetilde{\mathcal{M}}' \right) \widetilde{\Gamma}_n^{n'} - \kappa \left(-\mathcal{M} \pm \widetilde{\mathcal{M}} \right) \Gamma_n^{n'} \right] \right\}. \tag{93}
\end{aligned}$$

$$\begin{aligned}
& T_z(|1^\pm\rangle \rightarrow |2^\mp\rangle) \\
&= eA_\pm B'_\mp \int d^3\mathbf{r} \sin(kz) \sin(k'z) \sin(j\phi) \sin(j'\phi) \\
&\times \left\{ i \left(\mathcal{M}' \mp \widetilde{\mathcal{M}}' \right) \left(-\mathcal{M} \pm \widetilde{\mathcal{M}} \right) z [k'\kappa J_j(\kappa r) J_{j'}(\kappa' r) - k\kappa' J_{j+1}(\kappa r) J_{j'+1}(\kappa' r)] \right. \\
&+ \left. \frac{R_0}{2} \left[\kappa' \left(\mathcal{M}' \mp \widetilde{\mathcal{M}}' \right) J_{j+1}(\kappa r) J_{j'+1}(\kappa' r) - \kappa \left(-\mathcal{M} \pm \widetilde{\mathcal{M}} \right) J_j(\kappa r) J_{j'}(\kappa' r) \right] \right\} \\
&= \frac{e\alpha}{2} A_\pm B'_\pm \delta_{ll'} \left\{ i \left(\mathcal{M}' \mp \widetilde{\mathcal{M}}' \right) \left(-\mathcal{M} \pm \widetilde{\mathcal{M}} \right) \left[k'\kappa I_n^{n'} - k\kappa' \widetilde{I}_n^{n'} \right] I_z(\Delta m, M) \right. \\
&+ \left. \frac{\hbar R_0}{4} \delta_{mm'} \left[\kappa' \left(\mathcal{M}' \mp \widetilde{\mathcal{M}}' \right) \widetilde{I}_n^{n'} - \kappa \left(-\mathcal{M} \pm \widetilde{\mathcal{M}} \right) I_n^{n'} \right] \right\}. \tag{94}
\end{aligned}$$

C. Selection rules in $x + iy$ -direction

$$\begin{aligned}
& T_{x+iy}(|1^\pm\rangle \rightarrow |1^\pm\rangle) \\
&= eA_\pm A'_\pm \int d^3\mathbf{r} \sin(kz) \sin(k'z) \sin(j\phi) \sin(j'\phi) \\
&\times \left\{ \kappa\kappa' \left(-\mathcal{M} \pm \widetilde{\mathcal{M}} \right) \left(-\mathcal{M}' \pm \widetilde{\mathcal{M}}' \right) r e^{\pm i\phi} J_j(\kappa r) J_{j'}(\kappa' r) \right. \\
&+ \left[k\kappa' \left(-\mathcal{M} \pm \widetilde{\mathcal{M}} \right) \left(-\mathcal{M}' \pm \widetilde{\mathcal{M}}' \right) + 1 \right] r e^{\pm i\phi} J_{j+1}(\kappa r) J_{j'+1}(\kappa' r) \\
&- \left. iR_0\kappa' \left(-\mathcal{M}' \pm \widetilde{\mathcal{M}}' \right) e^{i\phi} J_{j+1}(\kappa r) J_{j'}(\kappa' r) \right\} \\
&= \frac{e\hbar}{2} A_\pm A'_\pm \delta_{mm'} \left\{ \kappa\kappa' \left(-\mathcal{M} \pm \widetilde{\mathcal{M}} \right) \left(-\mathcal{M}' \pm \widetilde{\mathcal{M}}' \right) I_\phi^\pm(\Delta l, L) J_{nl}^{n'l'} \right. \\
&+ \left[k\kappa' \left(-\mathcal{M} \pm \widetilde{\mathcal{M}} \right) \left(-\mathcal{M}' \pm \widetilde{\mathcal{M}}' \right) + 1 \right] I_\phi^\pm(\Delta l, L) \widetilde{J}_{nl}^{n'l'} \\
&- \left. iR_0\kappa' \left(-\mathcal{M}' \pm \widetilde{\mathcal{M}}' \right) I_\phi^\pm(\Delta l, L) \widetilde{K}_{nl}^{n'l'} \right\}. \tag{95}
\end{aligned}$$

-
- [1] M. Governale, B. Bhandari, F. Taddei, K.-I. Imura, and U. Zülicke, “Finite-size effects in cylindrical topological insulators,” *New J. Phys.* **22**, 063042 (2020).
- [2] L. Gioia, M. G. Christie, U. Zülicke, M. Governale, and A. J. Sneyd, “Spherical topological insulator nanoparticles: Quantum size effects and optical transitions,” *Phys. Rev. B* **100**, 205417 (2019).
- [3] K.-I. Imura, Y. Yoshimura, Y. Takane, and T. Fukui, “Spherical topological insulator,” *Phys. Rev. B* **86**, 235119 (2012).
- [4] Izrail Solomonovich Gradshteyn and Iosif Moiseevich Ryzhik, *Table of integrals, series, and products* (Academic press, 2014).